Resource

Molecular Cell

A Compendium of RNA-Binding Proteins that Regulate MicroRNA Biogenesis

Graphical Abstract

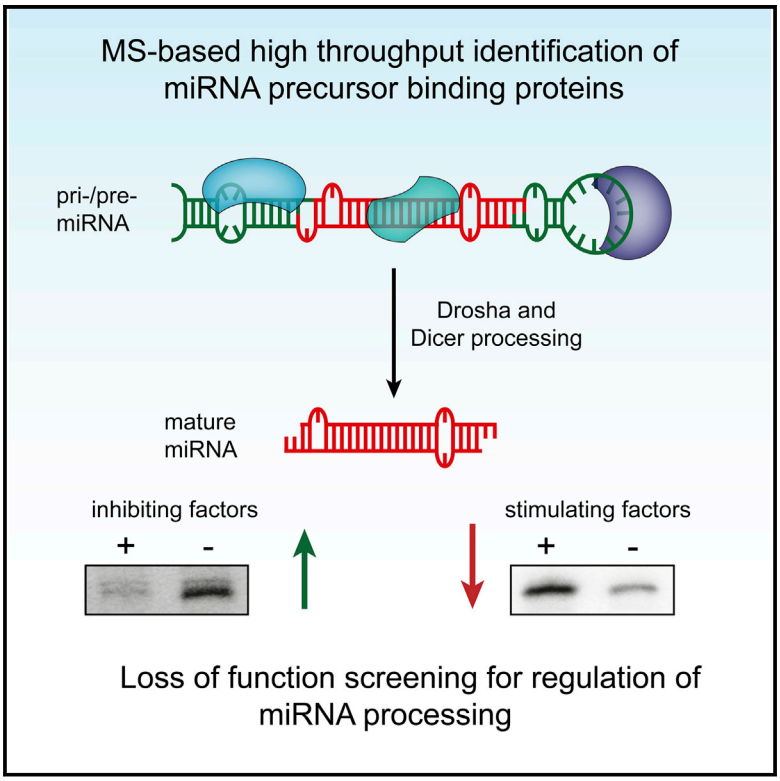

Authors

Thomas Treiber, Nora Treiber, Uwe Plessmann, ..., Kevin Schall, Henning Urlaub, Gunter Meister

Correspondence

gunter.meister@ur.de

In Brief

RNA-binding proteins (RBPs) can bind miRNA precursors and regulate their expression. Treiber et al. have identified protein interactors of more than 70 miRNA precursors in a large number of human cell lines. Depletion of distinct RBPs changes mature miRNA levels and thus indirectly modulates miRNA target mRNA expression levels.

Highlights

- A large-scale biochemical screen identifies a broad layer of RBP-miRNA interactions
- Loop and stem regions of miRNA precursors can specifically be recognized by RBPs
- Depletion of identified RBPs can positively or negatively affect miRNA levels
- RBPs can indirectly modulate mRNA expression by regulating mature miRNA levels

Treiber et al., 2017, Molecular Cell 66, 270–284
April 20, 2017
http://dx.doi.org/10.1016/j.molcel.2017.03.014

CellPress

CellPress

Molecular Cell
Resource

A Compendium of RNA-Binding Proteins that Regulate MicroRNA Biogenesis

Thomas Treiber,[1,3] Nora Treiber,[1,3] Uwe Plessmann,[2] Simone Harlander,[1] Julia-Lisa Daiß,[1] Norbert Eichner,[1] Gerhard Lehmann,[1] Kevin Schall,[1] Henning Urlaub,[2] and Gunter Meister[1,4,*]

[1]Biochemistry Center Regensburg (BZR), Laboratory for RNA Biology, University of Regensburg, 93053 Regensburg, Germany
[2]Bioanalytical Mass Spectrometry Group, Max-Planck-Institute of Biophysical Chemistry, 37077 Göttingen, Germany
[3]These authors contributed equally
[4]Lead Contact
*Correspondence: gunter.meister@ur.de
http://dx.doi.org/10.1016/j.molcel.2017.03.014

SUMMARY

During microRNA (miRNA) biogenesis, two endonucleolytic reactions convert stem-loop-structured precursors into mature miRNAs. These processing steps can be posttranscriptionally regulated by RNA-binding proteins (RBPs). Here, we have used a proteomics-based pull-down approach to map and characterize the interactome of a multitude of pre-miRNAs. We identify ~180 RBPs that interact specifically with distinct pre-miRNAs. For functional validation, we combined RNAi and CRISPR/Cas-mediated knockout experiments to analyze RBP-dependent changes in miRNA levels. Indeed, a large number of the investigated candidates, including splicing factors and other mRNA processing proteins, have effects on miRNA processing. As an example, we show that TRIM71/LIN41 is a potent regulator of miR-29a processing and its inactivation directly affects miR-29a targets. We provide an extended database of RBPs that interact with pre-miRNAs in extracts of different cell types, highlighting a widespread layer of co- and posttranscriptional regulation of miRNA biogenesis.

INTRODUCTION

MicroRNAs (miRNAs) are important regulators of gene expression and have not only been implicated in various different cellular pathways but also in embryonic development and tissue homeostasis (Bushati and Cohen, 2007). Animal miRNAs can be generated from introns of specific host pre-mRNAs, from individual genes and from larger clusters producing two to dozens of miRNAs (Bartel, 2009). After transcription, primary miRNA (pri-miRNA) transcripts contain hairpins, which are recognized by the microprocessor complex containing the RNase III DROSHA and the double-stranded (ds) RNA-binding protein (RBP) DGCR8. DROSHA cleaves off flanking single-stranded sequences and generates a miRNA precursor (pre-miRNA) that is transported to the cytoplasm (Kim et al., 2009). In the cytoplasm, the RNase III DICER1 binds pre-miRNAs and generates a ds miRNA intermediate from the stem of the pre-miRNA hairpin. With the help of the dsRBPs TRBP or PACT, one strand is selected and loaded into the RNA-induced silencing complex (RISC), where it directly interacts with a member of the Argonaute protein family (Dueck and Meister, 2014; Kim et al., 2009). The miRNA guides RISC to complementary sequences on target mRNAs, leading to their silencing or degradation (Jonas and Izaurralde, 2015).

MiRNA biogenesis is tightly regulated at all steps (Lin and Gregory, 2015). MiRNA transcription can be regulated by transcription factors that bind to specific promoters. Examples are the tumor suppressor TP53, which drives the expression of the miR-34 family (He et al., 2007; Raver-Shapira et al., 2007; Tarasov et al., 2007) or the oncogene MYC, which stimulates expression of oncogenic miRNAs such as the miR-17-92 cluster (He et al., 2005). Another example for regulation of miRNA expression and activity are posttranscriptional modifications of biogenesis factors and effector proteins, which may change their activity or specificity (Kim et al., 2010).

In recent years, it has become evident that the level of a mature miRNA is governed both by the transcription rate and the processing efficiency of the miRNA precursor by DROSHA and DICER1. This processing efficiency is, on the one hand, determined by structural and sequence features of the miRNA precursors that directly affect the processing machinery (Auyeung et al., 2013). On the other hand, specific RBPs can recognize sequences within miRNA precursors and modulate the processing efficiency depending on the cellular context or extrinsic signals (Choudhury and Michlewski, 2012; Connerty et al., 2016; Lin and Gregory, 2015). For example, the stem cell factor LIN28 interacts with the pre-miRNAs of most members of the let-7 family and blocks their expression (Newman et al., 2008; Rybak et al., 2008; Triboulet et al., 2015; Heo et al., 2008; Viswanathan et al., 2008). It recognizes sequence elements in the loop of pre-let-7 miRNAs and recruits the terminal uridyltransferases TUT4 or TUT7 to pre-miRNAs (Heo et al., 2009; Thornton et al., 2014). These enzymes add a short poly(U) tail to the 3′ end of the pre-miRNA and thus prevent further processing by DICER1. The poly(U) tail is recognized by the exonuclease DIS3L2 and the pre-miRNA is subsequently degraded (Chang et al., 2013; Faehnle et al., 2014). Interestingly, in the absence of LIN28 in non-stem cells, mono-uridylation mediated by TUT4, TUT7, and

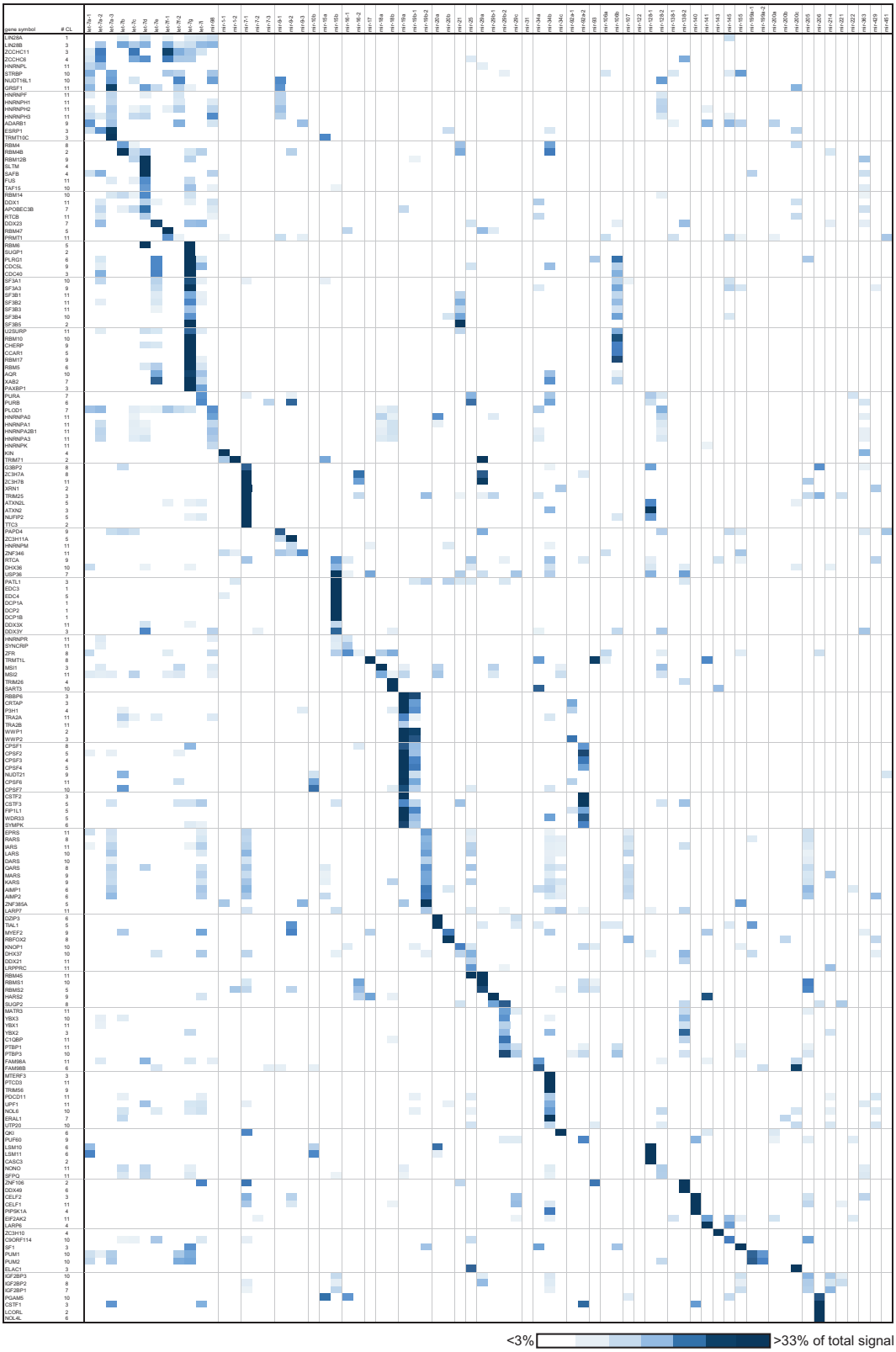

(legend on next page)

TUT2 promotes DICER1 processing of pre-let-7 members (Heo et al., 2012). In addition to LIN28, a number of other RBPs have been implicated in the regulation of miRNA processing, albeit with less clearly defined effects and functional relevance. For example, HNRNPA1 binds to pri-miR-18a and functions as auxiliary factor for DROSHA (Guil and Cáceres, 2007; Michlewski et al., 2010). Similarly, the KH-type splicing regulator KHSRP binds to the terminal loop of several miRNAs including let-7a and promotes processing (Trabucchi et al., 2009). Other examples for terminal loop binding proteins are MSI2 regulating miR-7 expression in the brain (Choudhury et al., 2013) or TDP43 that binds to sequence elements in the loop of pre-miR-143 and pre-miR-547 (Kawahara and Mieda-Sato, 2012).

Although a number of RNA-binding proteins have been implicated in miRNA biogenesis, a comprehensive picture of the dynamic interactome of pri-/pre-miRNAs is still missing. Toward such an interaction atlas, we have performed a biochemical screen using 72 different pre-miRNA baits, which were immobilized and incubated with lysates from 11 different cell lines. Specific protein interactors were identified by mass spectrometry and selected binding events were subsequently validated and further characterized. Furthermore, the functional relevance of the interactions were assessed by loss-of-function experiments, showing that a large number of the investigated candidates had an influence on the processing of the bound miRNA precursors under the conditions that we applied. Our results suggest that modulation of miRNA processing by specific RBPs is a widespread mechanism that may be relevant for a broad range of biological systems.

RESULTS

Systematic Analysis of Mature, Pri-miRNA, and Pre-miRNA Levels

To establish a comprehensive atlas of proteins that posttranscriptionally regulate miRNA biosynthesis, we designed a test set of 72 human miRNA precursors that includes miRNAs previously reported to be posttranscriptionally regulated, different precursors producing the same mature miRNAs (e.g., miR-7-1 to miR-7-3), and miRNAs organized in clusters (see the STAR Methods). In order to detect possible tissue- or tumor-specific regulatory mechanisms, we selected a panel of 11 cell lines covering a large variety of tissue origins (see the STAR Methods). Using different quantification approaches, we found that levels of processing intermediates can strongly vary between cell types suggesting a broad layer of posttranscriptional regulation (Figures S1A–S1D; Table S1). For example, the block of pre-let-7 family processing in stem cells by LIN28A can clearly be observed in the teratocarcinoma cell line NTERA-2 (Figure S1C, let-7g). In addition, let-7g processing is stalled in hepatocellular carcinoma (HEPG2) and neuroblastoma (SK-N-MC) cells, which express LIN28B. In contrast to inhibition of let-7g processing, enhanced mature miRNA levels are observed in the melanoma cell line SK-MEL-28 and in prostate carcinoma cells (DU145). Another example is miR-140 processing, which is reduced in MCF7 cells, while it is rather efficient in SK-N-MC cells (Figure S1C, miR-140). Similarly, miR-21 is more efficiently processed in colon cancer (DLD-1), HEPG2, and SK-MEL-28 cells than in other cell lines (Figure S1C, miR-21). Finally, miR-15 and miR-16 are transcribed in two pairs (miR-15a/miR-16-1 and miR-15b/miR-16-2), and a similar pattern of cell line-specific processing differences is observed for both loci (Figure S1D). Taken together, our results suggest that posttranscriptional regulation of miRNA processing is a widespread and cell-type-specific phenomenon (Table S1).

A Proteomics Approach to Identify miRNA Hairpin Binding Partners

In order to identify regulatory proteins that specifically interact with the 72 pre-miRNAs, we performed in vitro interaction studies. MiRNA hairpins containing a uniform 5′ extension were generated in vitro. Using a biotinylated 2′-O-methyl oligoribonucleotide complementary to the 5′ extension, the RNA was immobilized and incubated with lysates from the 11 different cell lines (Figure S1E). After washing, associated proteins were separated by SDS-PAGE and analyzed by mass spectrometry. Gel analysis before and after the pull-down confirms RNA integrity during the experiment (Figure S1F). A similar approach has been used before and led to the identification of LIN28 as let-7 pre-miRNA binder (Heo et al., 2008).

Our pull-down experiments yielded interaction data from 792 samples. The resulting comprehensive dataset allows for a clear distinction between background binders and specific protein-RNA interactions. Individual binding events were scored according to the enrichment of a given protein associated with a specific miRNA hairpin compared to all other precursors. Furthermore, the binding events were compared between the different cell lines and checked for consistent specificity. Factors that were exclusively identified in a single cell line are listed in Table S2 (see the STAR Methods).

In total, we identified 180 proteins that show preferential or specific binding to a single or a subset of miRNA precursors (Figure 1; Table S2). These include published regulators of miRNA biogenesis such as LIN28A/B, TUT4, and TUT7, which we find preferentially associated with let-7 family precursors, or RBPs such as HNRNPA1 (Guil and Cáceres, 2007) and YBX1 (Wu et al., 2015) attesting high reliability of our biochemical approach. Of note, almost every miRNA hairpin tested is specifically recognized by one or a small set of proteins.

Consistent with potential functions as regulators of miRNA biogenesis, 88.3% of the called hits (Figure 2A) are annotated as RNA-binding in the UNIPROT database. Additional 7 proteins

Figure 1. The Landscape of Specific miRNA Hairpin Binding Proteins

Interacting proteins were pulled out of cell extracts using immobilized RNA hairpins, which are indicated on top. Spectrum counts of mass spectrometry identifications of individual proteins (gene symbols on the left) are plotted as percentage of the total counts averaged over all cell lines in which the protein was identified. The number of cell lines, in which each protein was identified is given in the #CL column. Specific binding is shown as shades of blue ranging from white (<3% total counts) to dark blue (>33% of total counts).

See also Figure S1 and Tables S1 and S2.

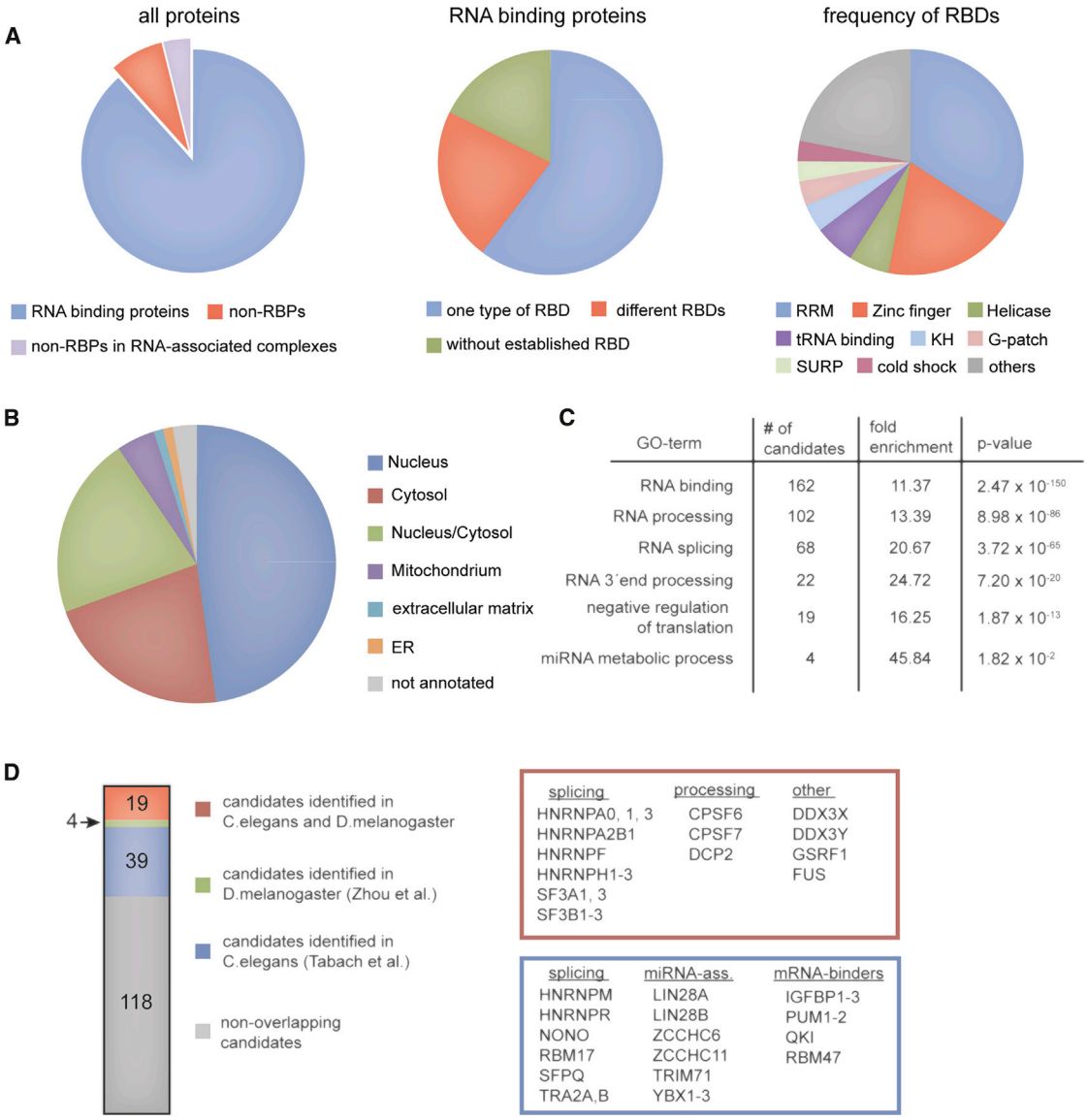

Figure 2. In Silico Analysis of Bound Candidates

(A) Classification of miRNA precursor binding proteins according to their reported RNA binding activity (left). Analysis of the abundance (middle) and type (right) of RNA binding domains of the candidates with reported RNA binding activity.

(B) Annotated subcellular localization of the candidate pri-miRNA binders.

(C) Enriched gene ontology terms of the miRNA hairpin binding candidates over all human genes.

(D) Overlap of the identified miRNA hairpin binders with putative small RNA pathway components from genetic analyses in *C. elegans* and *D. melanogaster*. All candidates orthologous to small RNA factors in both model organisms are shown in the red box. A selection of candidates orthologous to factors only identified in *C. elegans* is shown in the blue box. miRNA-ass, miRNA-associated.

See also Figure S2 and Table S3.

(3.9%) are non-RNA-binding components of RNA-associated complexes. Of the annotated RNA binders, 82% contain at least one domain with known RNA-binding function (Gerstberger et al., 2014) (Figure 2A). Interestingly, our dataset corroborates the RNA-binding capability of 28 proteins not harboring an established RNA-binding domain. Domains found in these proteins are listed in Table S3. Because our in vitro approach cannot distinguish between pri- and pre-miRNA binders, we assessed sub-cellular localization either by immunofluorescence staining of tagged proteins or by UNIPROT database analysis (Figures 2B and S2). We find that most proteins are either nuclear, which would suggest regulation on the pri-miRNA level, or cytoplasmic, hinting toward a function on DICER1 processing. A small subset of proteins localize to more distinct cellular compartments, suggesting potential background binding in our assay or pre-miRNA sequestration to distinct cellular sites. Further bioinformatic

assessment revealed that 162 out of our 180 candidates are associated with the GO-term "RNA binding" (Figure 2C). Others are associated with "RNA processing" or "splicing," indicating that our approach is specific toward RBPs and the background of non-RBPs is rather low. Finally, we compared our candidate list with screens for miRNA pathway candidates performed in flies (Zhou et al., 2008) or worms (Tabach et al., 2013). A total of 62 of our 180 candidates overlap with the published studies (Figure 2D). Many of the remaining candidates might engage in pri-/pre-miRNA-specific interactions, which may not have been analyzed in the published studies. In summary, our bioinformatic examination suggests a rather high level of true positive hits in our biochemical experiments.

Validation of Specific miRNA Hairpin-Protein Interactions

As a first validation step, we selected a set of candidates and expressed them as HA-tagged proteins in HEK293 cells. Repeating the miRNA precursor pull-down from cell lysates containing the overexpressed proteins followed by immunoblot against the HA-tag confirmed the binding specificity observed in our mass spectrometry analysis (Figure 3A). To further assess background-binding rates, we analyzed several candidates without a clear link to RNA-related processes. Among this small population, we still can confirm 30% of the candidates (Figure S3A). Useful antibodies against endogenous proteins were only available for a subset of candidates. Using these, we confirmed specific binding of several miRNA hairpins to RBM10, LIN28A, HNRNPA1, ZNF346, DDX21, and MATR3 (Figure 3B). We next analyzed association with precursors using RNA immunoprecipitation (RIP). As miRNA precursors are transient in nature and of low abundance, in many cases we could not reliably detect and quantify the endogenous pre-miRNA species. In order to still observe binding of candidate proteins to pre-miRNAs in cells, we co-transfected vectors expressing the pri-miRNA hairpin flanked by ~100 nt on both sides together with the FLAG-tagged candidates MATR3, ZNF346, and LIN28A. Indeed, pre-miR-29b-2 was detected by northern blot in anti-FLAG-MATR3, pre-miR-1-1 in anti-FLAG-ZNF346, and pre-let-7g in anti-FLAG-LIN28A immunoprecipitates (Figures 3C and S3B–S3D). No association was observed with mature miRNAs or a co-transfected control pre-miRNA. Additional candidates were examined by RIP followed by qPCR (Figure 3D). Although we find a broad range of recovery efficiency, binding is specific. Thus, using several different approaches, we confirmed a number of protein candidates suggesting a high level of specificity in our pull-down screen.

Characterization of RNA Determinants for miRNA Hairpin Recognition

In order to identify sequence regions and motifs on the miRNA hairpins that are contacted by RBPs, we analyzed binding to several miRNA hairpins in more detail (Figure 4). To this end, we constructed hybrid miRNA baits, in which the double-stranded stem and the single-stranded loop regions are exchanged between a binding and a non-binding precursor (Figure 4A, color code on top). These chimeric precursor molecules were used to pull down HA-tagged candidate proteins along with binding and non-binding control hairpins. The majority of the interactions can be mapped to the loop regions, in which a stretch of RNA sequence is single-stranded and exposed for base contacts ("loop binders"). When we searched the loop sequences of this set of precursors for the binding motifs of cognate protein partners, we found that known motifs were present in the apical loop regions (Figure 4B). Extending this search to the whole set of precursors, we frequently found that perfect or near-perfect motif matches in loop regions do not necessarily lead to specific binding thus demonstrating the need for a direct experimental assessment of recognition events (Table S4). However, if a motif-containing loop is bound, the motif is indeed essential for this interaction. For example, mutation of the AUCUU motif (Ray et al., 2013) in miR-29b-2 completely abolishes recognition by MATR3 (Figure 4C). Similarly, a weaker binding to pre-miR-138-2 is observed consistent with a mismatch in the binding motif. The interaction is strongly impaired upon further mutation of the motif (Figure 4C).

We also identified a set of proteins that bind to a specific pri-miRNA stem irrespective of the attached loop sequence (Figure 4A, "stem binders"). Among these proteins are the CUGBP Elav-like family members 1 and 2 (CELF1 and CELF2), for which a single-stranded recognition motif has been proposed consisting of $UGU(N)_{1-7}UGU$ (Edwards et al., 2011). Indeed, this motif is found in the lower stem region of the miR-140 precursor (Figure 4B), and mutation of any or both of the UGU motifs abolishes binding (Figure 4D). These findings suggest that specific single-stranded RBPs can break up the double-stranded stem of pri-miRNAs to liberate and bind their recognition sequences. ZNF346, which we identified as a stem-binding protein (Figure 4A), has been described as a dsRBP with no apparent sequence specificity (Burge et al., 2014). Nevertheless, we observe a clear binding preference for the three precursors of miR-9 and miR-155 (Figure 1). To further investigate this finding, we constructed truncated hairpin baits of miR-9-3 with deletions in different segments of the stem. This approach allowed us to narrow down the recognition site to an A/U-rich ds portion residing in the mature miRNA sequence (Figures 4E and S4A). Similarly, for miR-155, an A/U-rich stem region was found to be essential for binding (Figure S4B). Interestingly, mutations on one strand of this region in the miR-9-3 hairpin that break up two base pairs did not result in loss of binding, suggesting recognition independent of the ds structure (Figure 4E).

A single candidate in our test set—TRIM26—exhibited a more complex mode of recognition in which neither the stem nor the loop sequence was sufficient for binding (Figure 4A, "composite binder"). Interestingly, of all 72 miRNA precursors tested, TRIM26 binds exclusively to miR-18b, which differs in only three loop nucleotides from its paralog miR-18a. In order to identify the motif bound by TRIM26, we mutated these three positions individually or together to the corresponding sequence of miR-18a. Strikingly, every single mutation completely abolished binding (Figure 4F). Furthermore, an exchange of the stem sequence was only tolerated between the highly similar stems of miR-18a and miR-18b, whereas the complete loop region of miR-18b in context of the unrelated stem of miR-7-1 does not support binding (Figure 4F). Our data suggest a rather complex structural

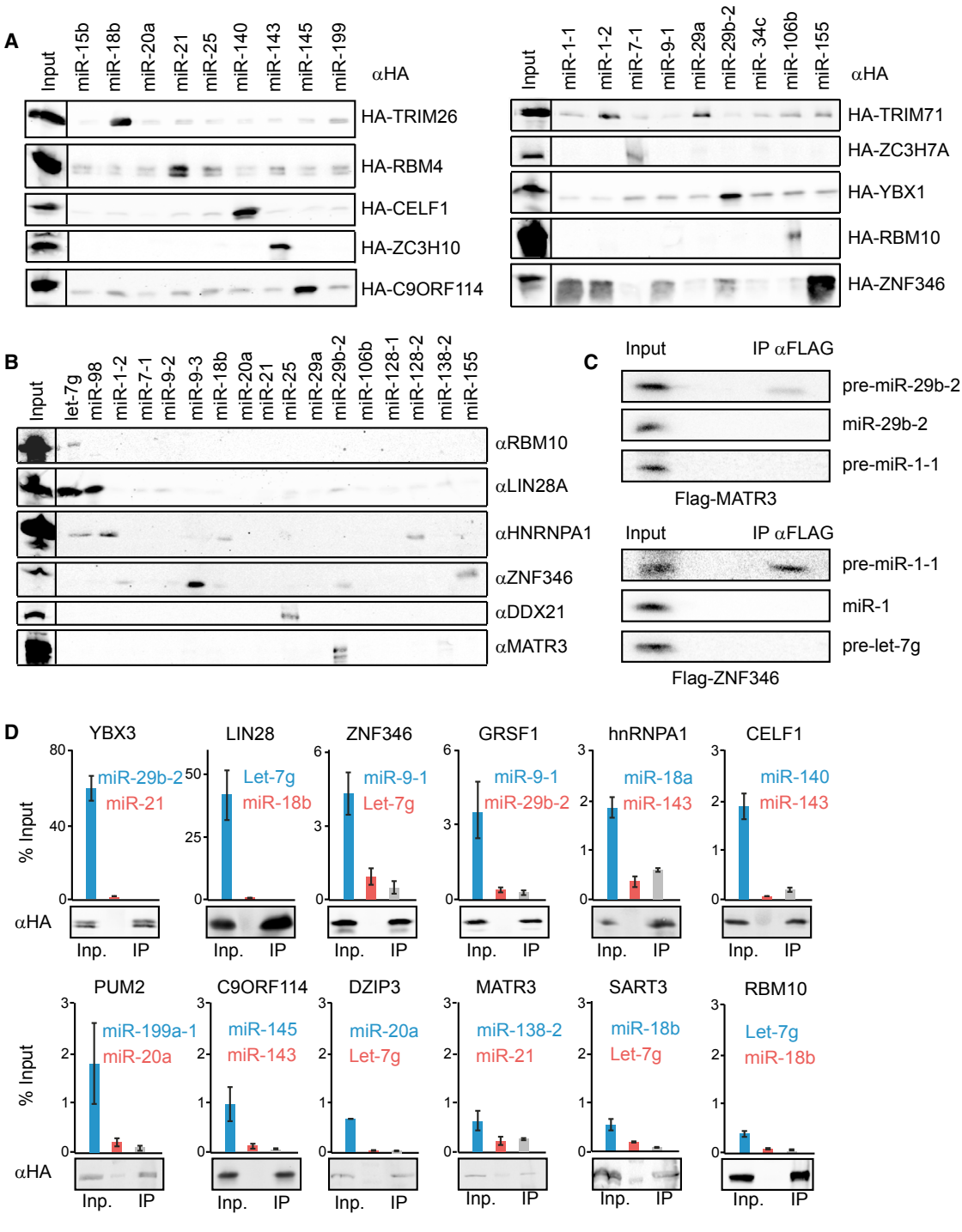

Figure 3. Validation of miRNA-Protein Interactions

(A) Pull-down of overexpressed HA-tagged candidate proteins using different miRNA hairpins. Eluate fractions and 4% of input material are analyzed by immunoblot against the HA-tag.

(B) RNA pull-down from Jurkat or NTERA-2 (for LIN28A) cell lysates using different miRNA hairpins. Eluate fractions and 4% of input material are analyzed by immunoblot using specific antibodies.

(C) RNA-IP assay from HEK cells overexpressing a Flag/HA-tagged candidate protein and two pri-miRNAs. Eluate fractions and 5% of input material are analyzed by northern blot (NB) using indicated antisense-RNA probes. Larger NB panels are shown in Figure S3.

(legend continued on next page)

arrangement necessary for the interaction of miR-18b with TRIM26.

Depletion of RBPs Affects miRNA Processing

Next, we investigated whether the miRNA-RBP interactions are indeed relevant for miRNA processing. For loss-of-function analysis, we used transient knockdown by RNAi or stable knockout cell lines created by CRISPR/Cas. Both methods are complementary but have nevertheless individual advantages and disadvantages, which often made only one of both approaches feasible for a given candidate protein.

C9ORF114 is a putative methyltransferase of the SPOUT-family and was reported to interact with mRNA (Baltz et al., 2012; Castello et al., 2012). In our screen, it exclusively bound the miR-145 hairpin (Figures 1 and 3A). As no homozygous knockout clones could be obtained (hinting at an essential role for this protein), we performed knockdown experiments using a specific siPool (Hannus et al., 2014) in HEPG2 cells. Three days after transfection, a consistent reduction of the mature miR-145 level by 35% could be observed by northern blot (Figure 5A). There was no decrease in the pri-miR-145 levels as measured by qPCR using primers detecting pri-miR-143 or pri-miR-145, which are synthesized as one primary transcript (Figure 5B) indicating posttranscriptional rather than transcriptional regulation by C9ORF114.

A pair of highly similar proteins identified in our screen are the two RBPs PUM1 and PUM2 (78% sequence identity), which we identified as miR-199a-1 and miR-199a-2 precursor binders (Figure 1). To elucidate the role of PUM1/2 in the processing of miR-199a, we introduced nonsense mutations into the individual *PUM* genes in HEK293 and SK-N-MC cells using CRISPR/Cas. As miR-199 is not expressed in HEK293 cells, we overexpressed a fragment of pri-miR-199a-1 along with pri-miR-143 as internal control and observed a reduced processing of miR-199a in two knockout lines for PUM1 and PUM2 (Figures 5C and S5A). Consistently, lower levels of endogenous miR-199a compared to an unrelated miRNA (miR-17) are present in one of two SK-N-MC PUM2 knockout clones and in both PUM1 knockout cell lines analyzed (Figure 5D). While strand-specific qRT-PCR failed to detect pri-miR-199a-1 expression, it revealed that pri-miR-199a-2 is mildly upregulated in the PUM1 or 2 knockout cell lines, indicating that the inhibitory effects on miR-199a maturation are posttranscriptional (Figure 5E). A direct effect of PUM1 is supported by filter binding assays in which the PUM-RBD specifically interacts with pre-miR-199a-1, but not pre-miR-145 (Figure 5F).

We further validated ZC3H7A and ZC3H7B, which are characterized by an array of three or four C3H zinc fingers interrupted by a C2H2 finger and followed by a short-coiled coil (Figure S5B). The two paralogs are 46% identical, and although mRNA association has been reported (Baltz et al., 2012; Castello et al., 2012), no recognition motifs have been described. We find an identical binding specificity of both proteins recognizing the hairpins of miR-7-1, miR-16-2, and weaker miR-29a (Figures 1 and 3A). Pull-down experiments with chimeric miRNA hairpins (Figure 5G) indicate that the ZC3H7 proteins recognize sequences in the apical loops. In order to identify critical bases for the interaction, we systematically mutated the short exposed apical sequence (5′-GATAAC-3′) of miR-7-1 and evaluated the binding activity of ZC3H7B to the mutant RNAs in pull-down assays (Figure 5H). Mutations of the central 5′-ATAA-3′ generally led to a strong reduction of binding with mutation to 5′-CTAA-3′ retaining full activity. In addition, mutation of the last A to other nucleotides only modestly reduced the amount of bound ZC3H7B. Accordingly, both miR-16-2 and miR-29a contain ATA(A/T) motifs in their terminal loops.

To assess functional importance of ZC3H7 proteins for miRNA biogenesis, we knocked out ZC3H7A in HEK293 cells and measured miR-7 and miR-16 levels by northern blot. MiR-29a is not detectably expressed in this cell line. In two independent knockout clones, we observed a partial loss of miR-7 compared to wild-type (WT) cells (Figure 5I). MiR-16 levels were not significantly altered. However, an increase in pre-miR-16 can be detected in the ZC3H7A knockout clones, which might suggest a delay in DICER1 processing (Figure S5C). The missing effect on mature miR-16 levels could be due to the fact that miR-16 is produced from two different genes (miR-16-1 and miR-16-2) but only miR-16-2 is bound by ZC3H7A (Figure S5D). The high conservation and identical binding specificity of ZC3H7A and B suggests that they could function redundantly in the regulation of miR-7-1. To test this, we knocked down ZC3H7B in WT and ZC3H7A knockout HEK cells (Figure S5E). Indeed, we observed a reduction of miR-7 levels also by loss of ZC3H7B and the phenotype of the ZC3H7A knockout is exacerbated by additional ZC3H7B knockdown. Pri-miRNA levels remain unchanged excluding transcriptional effects (Figures 5J and 5K). In summary, we have characterized ZC3H7A and ZC3H7B as specific regulators of miRNA biogenesis. Of note, we identified a total of 23 zinc-finger-containing proteins that selectively bind miRNA precursors suggesting that this might be an important protein class in this process.

The Nuclear RBP ZC3H10 Affects DROSHA Processing of pri-miR-143

In our proteomic screen, we identified a specific interaction between ZC3H10 and pri-miR-143 (Figures 1 and 3A). To elucidate the underlying molecular interactions, we mapped binding both on ZC3H10 and on pri-miR-143 (Figures 6A–6E). We systematically shortened ZC3H10 from the C terminus and performed pre-miR-143 pull-down experiments (Figure 6A). We find that all constructs interact, even the shortest one containing only the three zinc fingers, albeit less efficiently. Further mutation of the individual zinc fingers or combinations of zinc fingers show that the first two zinc fingers are essential for the interaction

(D) RNA-IP assays as described in (C) followed by qPCR analysis of the two cotransfected miRNA precursors and U1 small nuclear RNA (snRNA) as control for unspecific RNA binding. The expressed factors are indicated above the panels, the RNA bound in the pull-down screen is shown as blue, the control as red bar. Grey bars indicate the amount of co-immunoprecipitated U1 snRNA. Error bars give the SD of duplicate analyses. Immunoblots of input (1%) and precipitate (3%) are shown.
See also Figure S3.

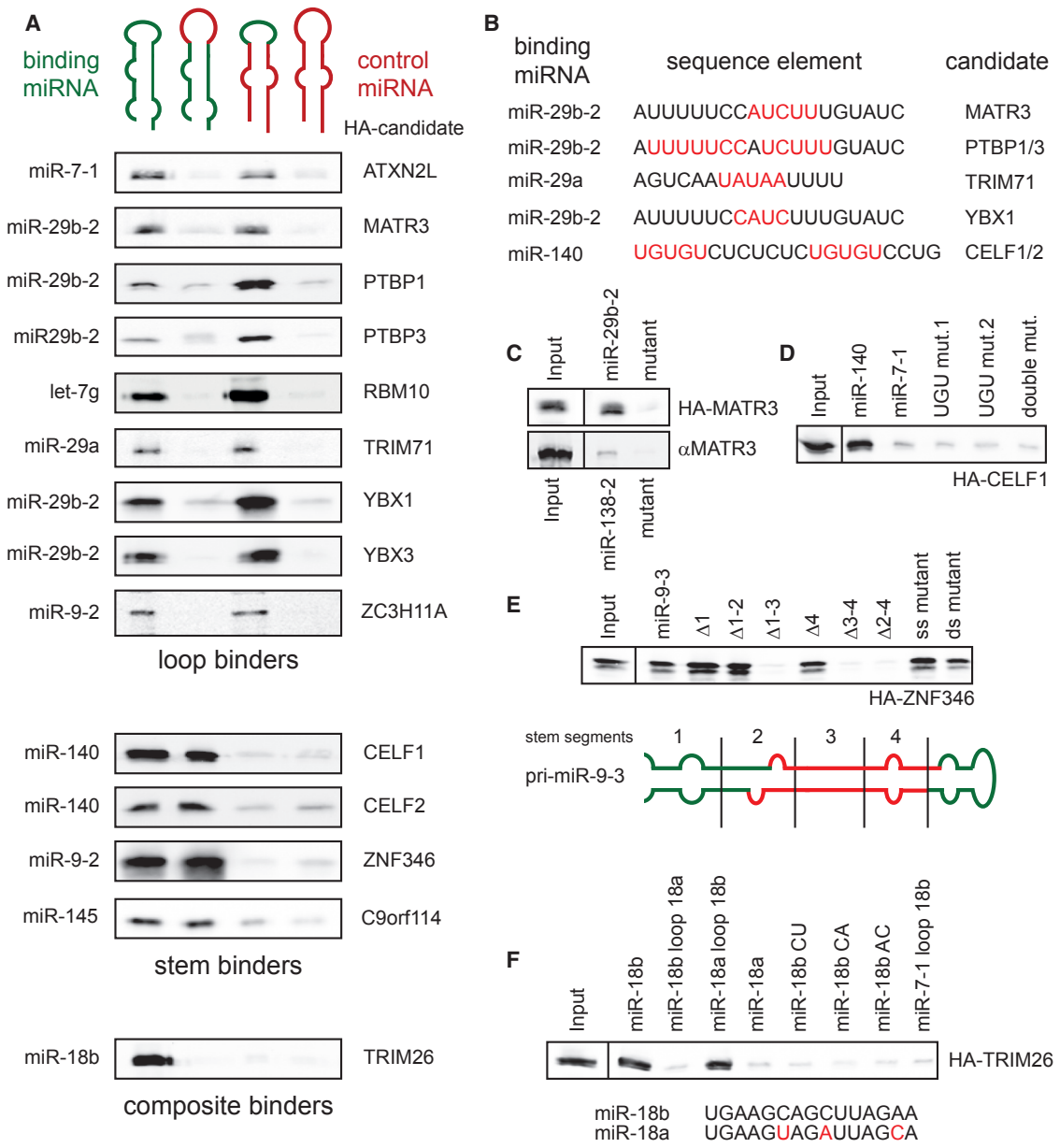

Figure 4. Loop and Stem Regions Serve as Specific Determinants of miRNA Hairpin Recognition

(A) Pull-down assay of overexpressed HA-tagged candidate proteins with chimeric miRNA hairpins. Loop and stem regions are exchanged between a pair of binding (as listed on the left) and non-binding RNAs (see the STAR Methods). Eluate fractions are analyzed by immunoblot against the HA-tag.

(B) Known recognition motifs of the candidate proteins analyzed in (A) are highlighted within the respective miRNA hairpin sequence. Except for the CELF proteins, for which the 5′ lower stem region is given, the loop sequences of the cognate miRNA hairpins are shown.

(C–F) Pull-down of overexpressed HA-tagged or endogenous candidate RBPs with different RNA baits; eluate fractions and 4% input are analyzed by immunoblot. (C) Pull-down of HA-MATR3 with the miR-29b-2 hairpin and a mutant hairpin containing a mutated recognition motif (top). Pull-down of endogenous MATR3 from NTERA-2-cells with the miR-138-2 hairpin and a hairpin containing a mutated binding motif; immunoblot with anti MATR3 antibody (bottom). (D) Pull-down of HA-CELF1 using the miR-140 hairpin and variants containing mutations in the two UGU motifs that constitute the CELF binding site. The pri-miR-7-1 hairpin is used as negative control. (E) RNA pull-down of HA-ZNF346 protein with different truncations of the miR-9-3 hairpin stem. Mutations destabilizing the double helix in segment 3 (ss mutant) and a compensating mutation on the opposite strand (ds mutant) are also tested. A schematic drawing of the miR-9-3 hairpin (mature miRNA shown in red) illustrates the deleted stem segments. For detailed sequence information on the used constructs see Figure S4A. (F) RNA pull-down of HA-TRIM26 with variants of the miR-18b hairpin. In an alignment of the loop sequences of miR-18b and miR-18a, the three variant positions, which are tested as point mutations in the pull-down assay, are highlighted.

See also Figure S4 and Table S4.

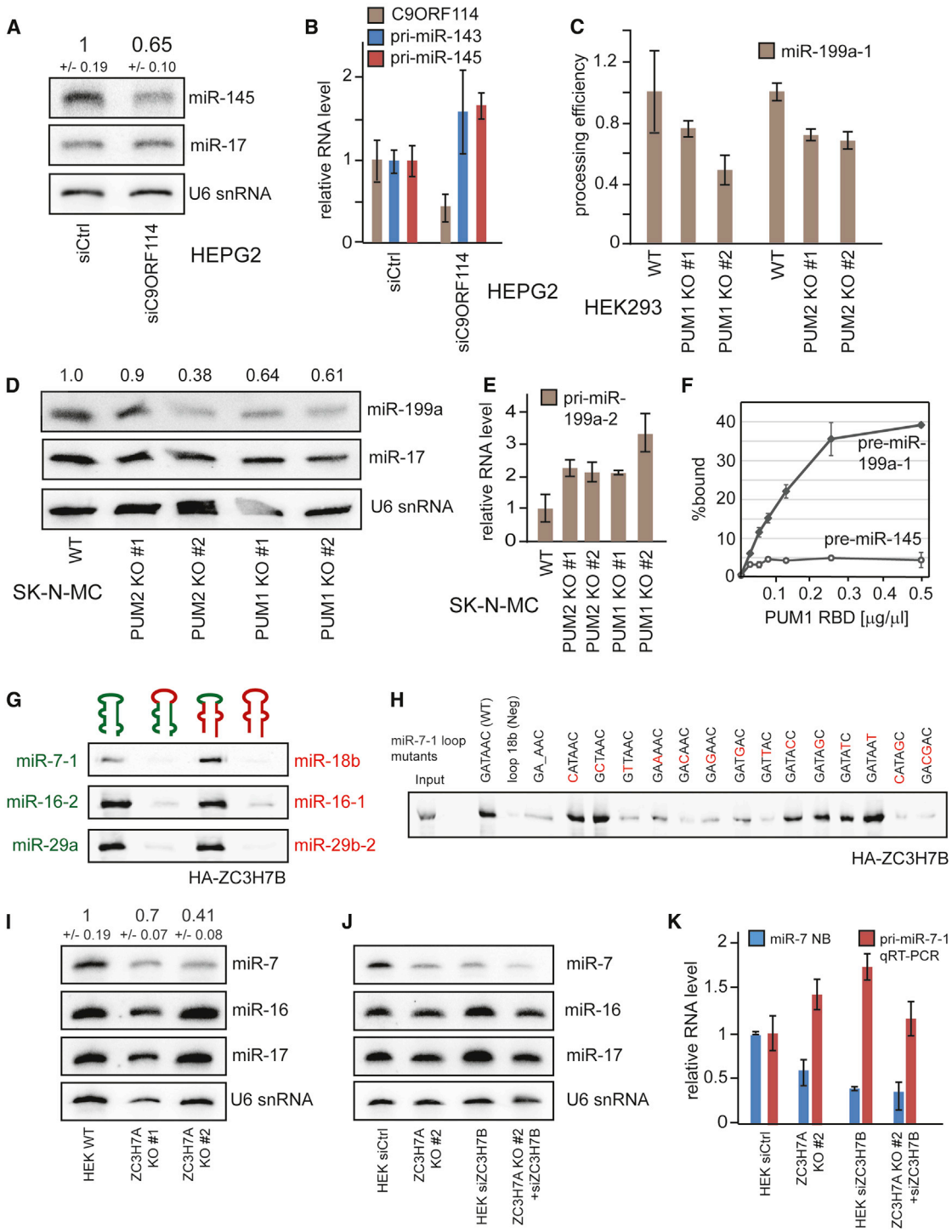

Figure 5. miRNA Precursor Binding Proteins Modulate Levels of Mature miRNAs

(A) NB analysis of HEPG2 cells transfected with C9ORF114-specific siRNAs or control siRNAs. The unrelated miR-17 and U6 snRNA are shown as loading controls. Quantitation of the relative level of miR-145 normalized to the signal for U6 snRNA are given above the lanes. Values represent the mean and SD of three experiments.

(B) qRT-PCR measurement of the C9ORF114 mRNA and miR-143/145 primary transcript.

(C) Overexpression of pri-miR-199a-1 in HEK cells or HEK cells with inactivated *PUM1* or *PUM2* genes. Levels of mature miRNAs are measured by NB and normalized to a co-transfected internal control (pri-miR-143). Error bars represent the SD of three experiments.

(legend continued on next page)

(Figure 6B). On the RNA side, pull-down experiments with hybrid hairpins exchanging the loop and stem regions of miR-143 and miR-145 show that the stem and not the loop of pri-miR-143 is recognized (Figure 6C). To further narrow down the binding region, truncated pri-miR-143 hairpins were used. Removal of the basal segment abrogated binding whereas shortening of the apical region had no effect (Figures 6D and S6A). For ZC3H10, the binding motif 5′-GCAGCGC-3′ was reported (Ray et al., 2013) and strikingly, a perfect motif match is present in the 5′ lower stem (red). Consistently, mutation of the motif disrupted the interaction with ZC3H10 protein (Figure 6D). To test if this interaction is direct, we performed electromobility shift assays (EMSAs) (Figure 6E). Indeed, an RNA containing the motif is efficiently shifted while the opposing sequence within the miR-143 stem is not, confirming direct interaction of ZC3H10 with pri-miR-143.

Overexpressed HA-ZC3H10 localizes to the nucleus (Figure S2), which would be in line with binding to the basal stem of pri-miR-143 and influencing microprocessor cleavage. To test whether ZC3H10 could be a regulator of miR-143 processing, we performed loss-of-function experiments. As CRISPR/Cas9-mediated genome editing did not yield homozygous knockouts in any of the cell lines tested, we treated heterozygote mutant SK-N-MC cells with small interfering RNA (siRNA) pools against ZC3H10, which indeed resulted in a strong upregulation of miR-143 (Figure 6F). Quantitation in three different clonal lines showed a 4- to 7-fold increase in the mature miRNA levels (Figure 6G), while qRT-PCR analysis confirmed an efficient knockdown of ZC3H10-mRNA and no upregulation of pri-miR-143/145 transcripts ruling out transcriptional effects (Figure 6H). Upregulation of miR-143 was also observed in NTERA-2 cells (Figure S6B) showing that the mechanism is not restricted to a single cellular background.

Similarly to ZC3H10, CELF1 and CELF2 are stem-binding candidates identified in our screen (Figure 4A). These two nuclear RBPs share 80% sequence identity, and while CELF1 appears to be ubiquitously expressed, CELF2 shows a more tissue-specific expression (Good et al., 2000). Both proteins bind to pri-miR-140, and simultaneous knockdown of CELF1 and CELF2 in SK-MEL-28 cells leads to a marked increase in miR-140 levels (Figure 6I), which is consistent with an inhibitory effect of CELF1/2. In line with a higher processing activity in CELF1/2 knockdown cells, the level of unprocessed pri-miR-140 is modestly reduced (Figure 6J). Single knockdown of CELF1 or CELF2 did not result in a significant change of miR-140 levels, hinting at a redundant role of the two family members in SK-MEL-28 cells (data not shown). Our data suggest that the nuclear RBPs CELF1/2 may act on the level of DROSHA processing as well.

TRIM71 Downregulates TET Proteins via miR-29a

The tripartite motif-containing protein TRIM71 is the human homolog of the *C. elegans* protein LIN-41. It was first identified as a target of let-7 miRNAs and is linked to the function of LIN28, which enables its expression by blocking let-7 biogenesis (Slack et al., 2000). TRIM71 was recognized as RBP that specifically contacts RNA via its C-terminal NHL-domain (Loedige et al., 2015).

TRIM71 selectively binds to the miR-1-2 and miR-29a hairpins in the LIN28-positive cell lines NTERA-2 and HEPG2 (Figure 1). For pri-miR-29a, binding was mapped to the apical loop (Figure 4A). To assess the potential regulatory function of this interaction, we performed knockdown experiments of TRIM71 in NTERA-2 cells and observed a modest but clear reduction of miR-29a levels by northern blot (Figure 7A). We therefore inactivated TRIM71 by CRISPR/Cas9 in NTERA-2 using two different guide RNAs (gRNAs). As shown by western blot analysis, TRIM71 expression is completely abrogated by the introduced nonsense mutations, while the cells retain their stem cell identity and express LIN28A at unchanged levels (Figure 7B). miRNA sequencing from TRIM71 knockout as well as WT cells revealed an overall unperturbed miRNA repertoire (Pearson's correlation >0.99). Notable exceptions are the downregulation of miR-29a (4.6-fold), which is consistent with the data from the knockdown experiment, and miR-100 (12.7-fold). On the other hand, miR-184 (15-fold) and miR-205 (7.3-fold) are upregulated compared to WT levels (Figure 7C). Northern blot analysis confirms these results (Figure 7D). In order to check if additional deregulated miRNAs apart from miR-29a might be directly bound by TRIM71, we performed pull-down assays using the corresponding miRNA hairpins. MiR-184 showed no binding of TRIM71 and even including 100 nucleotides of up- and downstream sequence in the miR-184 pull-down did not lead to an association with TRIM71 indicating an indirect effect of TRIM71 loss on this miRNA. In contrast, the miR-100 bait was bound by TRIM71 (Figure 7E) suggesting that direct regulation

(D) NB analysis of mature miR-199a, miR-17 and U6 snRNA in SK-N-MC cells and derived clonal lines with inactivated *PUM* genes. A quantitation of the miR-199a level normalized to miR-17 is given above the lanes.
(E) qRT-PCR measurement of the miR-199a-2 primary transcript of the cell lines shown in (D).
(F) Filter binding assay of ^{32}P-labeled pre-miR-199a-1 and pre-miR-145 pre-incubated with increasing amounts of purified PUM1 RBD. The percentage of RNA recovered is plotted against the protein concentration. Error bars indicate the SD of two experiments.
(G) Pull-down of HA-ZC3H7B protein using chimeric miRNA hairpins in which stem and loop segments of a binding miRNA (indicated in green) and non-binding miRNA (indicated in red) are exchanged.
(H) Pull-down of HA-ZC3H7B protein with mutant versions of the miR-7-1 hairpin. Eluate fractions and 4% input are analyzed by immunoblot against the HA-tag. Loop sequences are shown above the respective lanes and mutations compared to the WT sequence are highlighted in red.
(I) NB analysis of indicated miRNAs and U6 snRNA in HEK cells and two ZC3H7A knockout lines. A quantification of the miR-7 level normalized to U6 snRNA is indicated above the lanes. Larger NB panels are shown in Figure S5C.
(J) Knockdown of ZC3H7B in WT and ZC3H7A-deleted HEK cells. NB probes are indicated.
(K) Quantitation of mature miR-7 levels by NB (blue) and pri-miR-7-1 levels by qRT-PCR (red) in ZC3H7B knockdown and control samples. Error bars indicate the SD of triplicate experiments.
See also Figure S5.

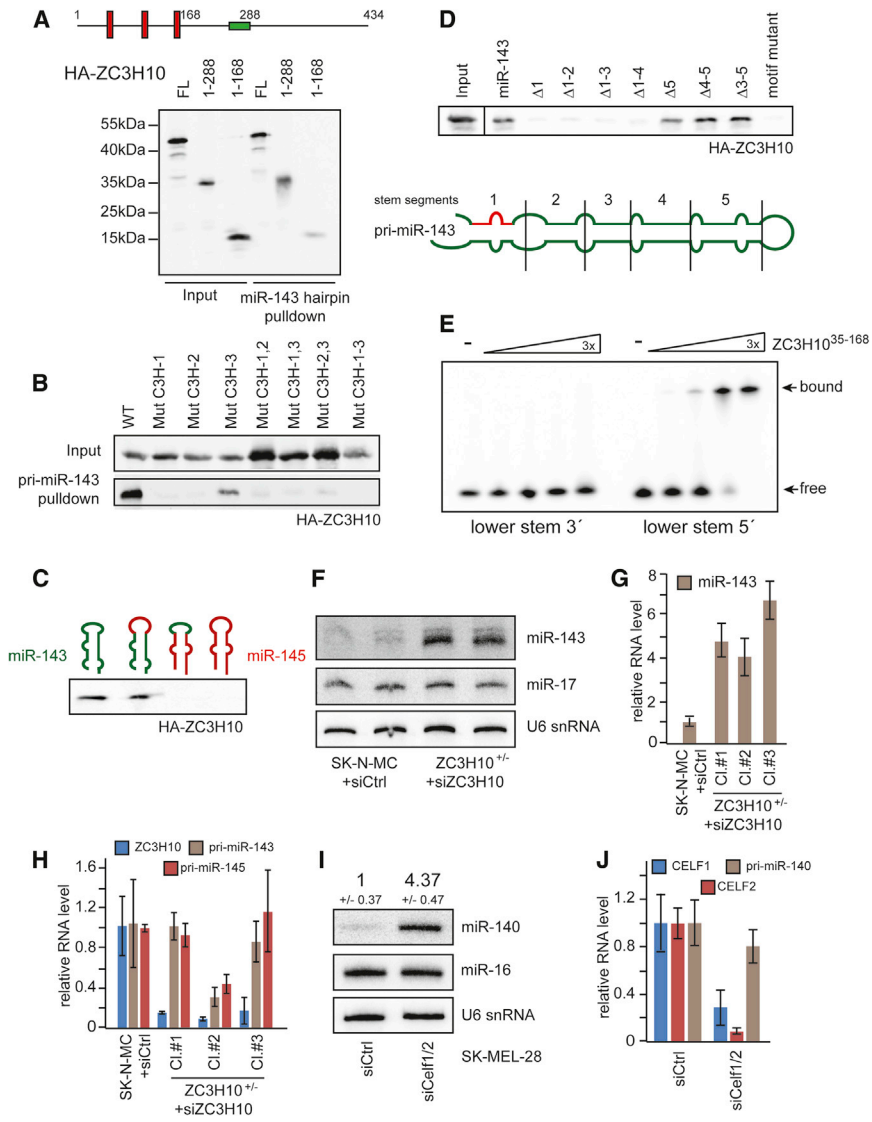

Figure 6. The Basal Stem Binders ZC3H10 and CELF1 Inhibit miRNA Processing

(A) Schematic representation of the ZC3H10 protein. The three zinc fingers are shown as red boxes, the coiled-coil region is marked in green. The positions of C termini of truncated versions are indicated. HA-tagged full-length ZC3H10 protein and two truncated constructs are compared in an RNA pull-down assay with the miRNA-143 hairpin. In (A)–(D), eluate fractions and, if applicable, 4% input are analyzed by immunoblot against the HA-tag.

(B) Pull-down of overexpressed HA-ZC3H10 proteins with mutated Zn^{2+}-chelating residues of different zinc fingers.

(C) Pull-down of overexpressed HA-ZC3H10 protein with chimeric RNA hairpins in which stem and loop segments of a binding miRNA (indicated in green) and non-binding miRNA (indicated in red) are exchanged.

(D) RNA pull-down of overexpressed HA-tagged ZC3H10 protein using different truncations of the miR-143 hairpin stem. A hairpin carrying a mutation of a putative recognition motif is also tested. A schematic drawing of the miR-143 hairpin illustrates the deleted stem segments with the mutation highlighted in red. For detailed sequence information on the used constructs, see Figure S6A.

(E) Gel shift assay using labeled 9-mer RNA oligonucleotides corresponding to both strands of the pri-miR-143 basal stem region. Increasing addition of purified ZC3H10 (0.1−3 μM) as well as the positions of free and bound RNA are indicated.

(F) NB analysis of miR-143, miR-17, and U6 snRNA in SK-N-MC cells transfected with control siRNAs and heterozygous SK-N-MC cells transfected with ZC3H10-specific siRNA.

(G) Quantitation of NB experiments as described in (F) performed in three independent heterozygote cell lines. MiR-143 levels normalized to the U6 snRNA signal are shown, error bars indicate the SD of triplicate transfections.

(H) qRT-PCR analysis of ZC3H10 mRNA and pri-miR-143/145 levels of ZC3H10 and control knockdown samples.

(I) NB analysis of SK-MEL-28 cells transfected with CELF1- and CELF2-specific siRNAs or control siRNAs. Quantitation of the relative level of miR-140 normalized to the signal for U6 snRNA are given above the lanes. Values represent the mean and SD of two experiments.

(J) qRT-PCR measurement of the miR-140 primary transcript as well as the mRNAs of CELF1 and CELF2.

See also Figure S6.

by TRIM71 is not restricted to miR-29a. Importantly, levels of pri-miR-29a are not downregulated in the knockout clones (Figure 7F) confirming posttranscriptional regulation.

The ten-eleven translocation (TET) family of cytosine demethylases (TET1–TET3) is predicted to be regulated by miRNA-29a as the 3′ UTRs of the TET1-3 mRNAs contain multiple conserved target sites (Agarwal et al., 2015) (Figure 7G). Furthermore, TET1 has recently been reported to collaborate with LIN28 in the regulation of transcription (Zeng et al., 2016). This led us to test whether inactivation of TRIM71 and the resulting downregulation of miR-29a leads to derepression of TET mRNAs. Indeed, TET2 and TET3 mRNA levels are increased in TRIM71 knockout cells while TET1 levels remain unchanged (Figure 7G), probably reflecting the presence of fully seed-matched target sites in these two mRNAs. Strikingly, inhibition of miR-29a in WT cells using a 2′-O-methylated antisense inhibitor copies the phenotype of the TRIM71 knockout cells and increases the levels of TET2 and 3 but not TET1 (Figure 7H). These findings highlight that modulation of miRNA levels through posttranscriptional regulators can directly impact target gene expression.

DISCUSSION

miRNAs are frequently organized in genomic clusters or transcribed together with a protein coding host gene, which limits the flexibility of transcriptional control mechanisms.

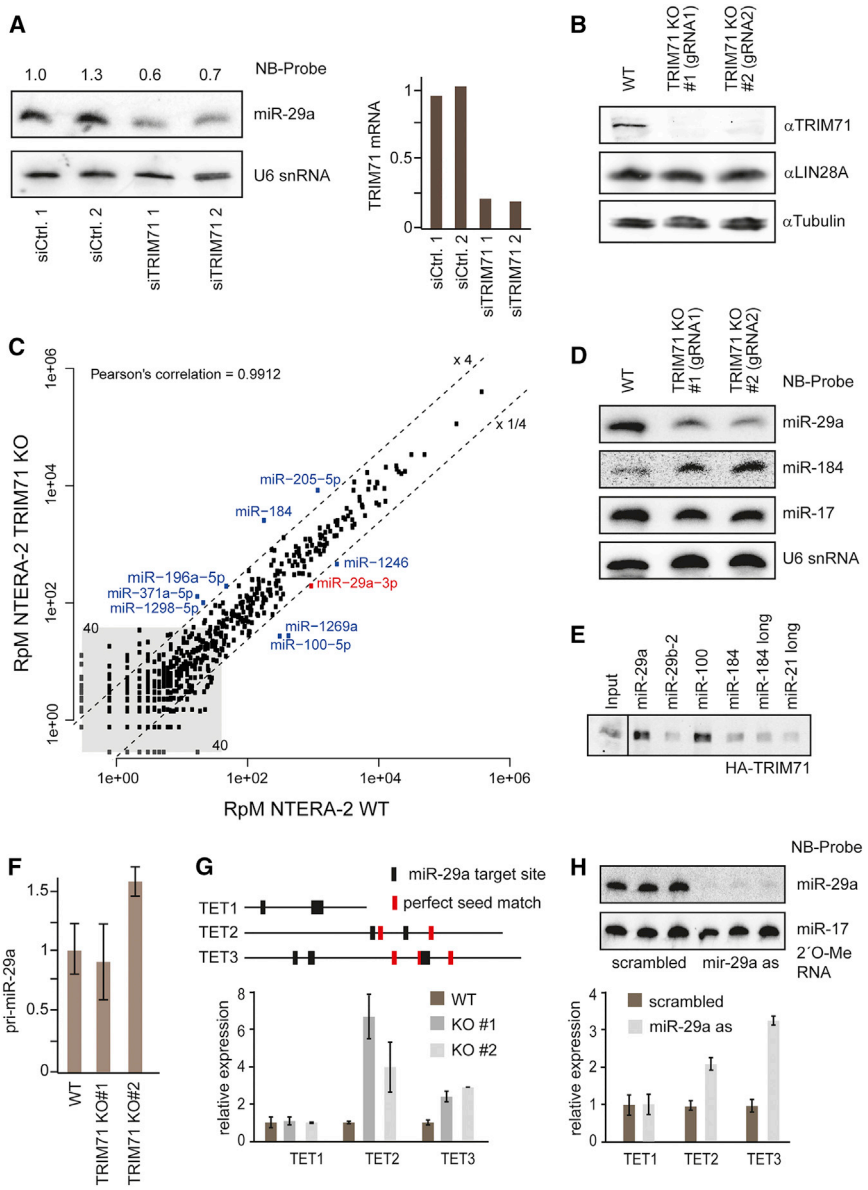

Figure 7. TRIM71 Regulates miRNA-Mediated Gene Silencing Independent of LIN28

(A) siRNA-mediated knockdown of TRIM71 in NTERA-2 cells. Levels of miR-29a and U6 snRNA are analyzed by NB, normalized miR-29a levels are shown on top. TRIM71 mRNA is measured by qRT-PCR.

(B) Western blot analysis of NTERA-2 cells and two derived cell lines carrying nonsense mutations in the *TRIM71* gene.

(C) Scatterplot of miRNA read numbers from deep sequencing libraries derived from NTERA-2 cells (x axis) and the mean of two *TRIM71* knockout cell lines (y axis). miRNAs more than 4-fold up- or downregulated in the knockouts are labeled, miR-29a is highlighted in red.

(D) NB analysis of WT and TRIM71-deficient NTERA-2 cells; used probes are indicated.

(E) Pull-down of overexpressed HA-tagged TRIM71 protein using hairpins of deregulated miRNAs. Eluate fractions and 4% input are analyzed by immunoblot against the HA-tag. Baits labeled as long (miR-184 long and miR-21 long as control) contain additional 100 nt on either side of the hairpin structure.

(F) qRT-PCR analysis of pri-miR29a in NTERA-2 cells and the TRIM71-deficient clonal lines. Error bars indicate SD of two cDNA syntheses.

(G) Schematic representation of the 3′ UTR regions of the *TET1-3* genes. MiR-29a target sites are indicated as boxes. Red boxes highlight perfect 8-mer seed matches. mRNA levels of TET1-3 in TRIM71 proficient and deficient NTERA-2 cells are measured by qRT-PCR. Error bars indicate SD of two cDNA syntheses.

(H) Inhibition of miR-29a by antisense 2′-O-methyl RNA transfection in NTERA-2 cells. Northern blot analysis of miR-29a and miR-17 as unrelated control are shown. qPCR of TET1-3 was performed for triplicate experiments. Relative transcript abundance and the SD are indicated.

Consequently, since the discovery of LIN28 it has become increasingly clear that posttranscriptional events play an important role in shaping the cellular miRNA repertoire. While for larger miRNA clusters RNA-folding and thus differential accessibility of the miRNAprocessing machinery is important (Contrant et al., 2014; Du et al., 2015), processing of individual miRNA transcripts can be influenced by RBPs (Treiber et al., 2012).

To identify RBPs that contribute to miRNA processing, we performed a comprehensive screen for binders of immobilized miRNA hairpins. Although our screen is performed in vitro and one would expect significant background binding activity, the large dimension of our approach allows for a clear distinction between specific and unspecific binding. In fact, we find mainly one and sometimes a few RBPs that specifically interact with a given pre-/pri-miRNA. However, it should be noted that in vitro approaches might also identify unphysiological binding for example due to high bait concentrations, a potential lack of cell compartmentalization, or a specific RNA history that is required for physiological binding. Based on our mass spectrometry analyses, we provide an extended protein interactome database for 72 miRNA hairpins in 11 different cell lines. Besides the LIN28-TUT4/7 axis, several other RBPs have been implicated in the regulation of miRNA biogenesis. Many of these factors are also among our identified proteins including HNRNPA1 that regulates the expression of pre-miR-18a (Guil and Cáceres, 2007). Although rather modest, our proteomics data confirm binding of HNRNPA1 to miR-18a. In addition, we find specific interactions with let-7 family members (e.g., miR-98) or miR-128-2. Interestingly, we observed binding of other HNRNPA paralogs (HNRNPA0, HNRNPA2B1, or HNRNPA3) to the same hairpins indicating that protein paralogs can function redundantly, which needs to be considered for interpretation of validation data. Similarly, YBX1 has been

implicated in miR-29b-2 processing (Wu et al., 2015). Our screen confirms this interaction and shows additional interaction with the miR-138-2 hairpin. This binding is shared by all three human paralogs (YBX1–YBX3) indicating a broader regulatory role of YBX proteins in miRNA biogenesis. Importantly, the initial evidence for a role of HNRNPA and YBX1 in miRNA regulation came from CLIP-data that showed in vivo binding of these proteins to pre-miRNA sequences. Our in vitro pull-down experiments faithfully reproduce these interactions, demonstrating the potential to capture regulatory proteins even without cross-linking.

Several other RBPs that were reported to regulate pre-miRNA processing are also found in our analyses but associate with different pre-miRNAs. For example, TRIM25 has been reported to regulate let-7 expression (Choudhury et al., 2014), whereas we find that it binds specifically to miR-7. Similarly, MSI1/2 were proposed to regulate miR-7 expression (Choudhury et al., 2013) but we observe strong binding to pre-miR-18a and pre-miR-20a. Still other factors, which have been implicated in pre-miRNA processing, such as KHSRP (Trabucchi et al., 2009) or SmD1 (Xiong et al., 2015), were not among the specific binders in our screen. This might be due to the different systems that have been studied or different stringencies that were applied to experimental conditions and data analysis. Finally, factors such as SMAD proteins (Davis et al., 2008) are not identified at all, which is not surprising as SMAD proteins have to be activated by extracellular signals. This illustrates that some regulatory mechanisms are very specific to cell types and/or physiological environments. While we tried to cover a broad range of human tissues by selecting various cell lines, some binding events seen in our screen might only be relevant in a particular cell type and under specific conditions. Furthermore, many of the factors investigated by us and others show only moderate effects on mature miRNA levels, consistent with our profiling analysis of miRNA and precursor levels. For functional validation of our identified miRNA binders, we used transient knockdown and/or stable knockout. For knockdown experiments, timing might be critical because both protein and miRNA pools might have low turnover rates. On the other hand, creating stable knockout cells using CRISPR/Cas is not feasible for essential proteins and very complex for a group of homologous binders that might have redundant functions. In addition, adaptation processes can lead to a large variability between different clonal knockout lines.

Many of the identified RBPs have been characterized in different pathways and may fulfill housekeeping functions. Among the specific pre-miRNA binders, we find candidates that are involved in mRNA capping, splicing or 3′ end processing (Figure 2C). All these processes are tightly linked to transcription and influence each other. Because it has been shown that DROSHA processing occurs co-transcriptionally as well (Ballarino et al., 2009), it is tempting to speculate that general mRNA processing components actively stimulate or repress pri-miRNA processing already during RNA polymerase II transcription. This could be particularly important for clustered miRNAs or miRNAs that are part of introns of host genes. Consistently, it has been reported in *C. elegans* that miRNAs have co-evolved with intron splicing (Tabach et al., 2013). Because a general functional correlation between a host gene and an intron-residing miRNA, for example, has not been observed, RBPs that are involved in both pathways might be able to separate mRNA from miRNA expression. Such general RBPs might function as coordinators regulating accurate levels of distinct RNA species. In agreement with such a scenario, the RBP FUS appears to recruit DROSHA to distinct pre-miRNA loci co-transcriptionally (Morlando et al., 2012).

STAR★METHODS

Detailed methods are provided in the online version of this paper and include the following:

- KEY RESOURCES TABLE
- CONTACT FOR REAGENT AND RESOURCE SHARING
- EXPERIMENTAL MODEL AND SUBJECT DETAILS
- METHOD DETAILS
  - Pri-miRNA Screening by qPCR
  - Profiling of microRNAs by Northern Blot
  - Profiling of Mature miRNAs by Deep Sequencing
  - Generation of hairpin baits for RBP-Pull-down
  - Pull-down of miRNA hairpin-binding Proteins
  - Mass Spectrometry Analysis
  - Analysis of Mass Spectrometry Data
  - Data base analysis of candidate proteins
  - Verification and Analysis of Binding Events
  - Western Blotting
  - RNA Immunoprecipitation (RIP)
  - Poly-A-Tailing and RT- qPCR analysis
  - Genome Editing Using CRISPR/Cas9
  - Analysis of Clones from CRISPR/CAS9 editing
  - Gene Knockdown by siRNA Pools
  - Processing Assay of pri-miRNAs in KO Lines
  - Mapping of ZC3H10:pri-miRNA-143 interaction
  - Purification of recombinant ZC3H10
  - Electrophoretic Mobility Shift Assay (EMSA)
  - miRNA-Inhibitor Assay
  - Purification of recombinant PUM1 protein
  - Filter Binding Assay
  - qRT-PCR Analysis of Specific mRNAs
  - Immunofluorescence
- QUANTIFICATION AND STATISTICAL ANALYSIS
- DATA AND SOFTWARE AVAILABILITY

SUPPLEMENTAL INFORMATION

Supplemental Information includes six figures and six tables and can be found with this article online at http://dx.doi.org/10.1016/j.molcel.2017.03.014.

AUTHOR CONTRIBUTIONS

N.T. and T.T. conceived the study, performed experiments, analyzed data, and wrote the manuscript. U.P. and H.U. performed mass spectrometry analyses. S.H., J.-L.D., and K.S. performed experiments. N.E. and G.L. generated and analyzed deep sequencing data. G.M. supervised the project, interpreted data, and wrote the manuscript.

ACKNOWLEDGMENTS

We thank S. Ammon and C. Friederich for technical assistance and support and G. Wulczyn for reagents. Our research is supported by grants from the DFG (SFB960, SPP1935), the European Research Council (ERC grant "moreRNAs"), and the Bavarian Systems-Biology Network (BioSysNet). G.M. is a co-founder of siTOOLs Biotech.

Received: August 5, 2016
Revised: December 22, 2016
Accepted: March 20, 2017
Published: April 20, 2017

REFERENCES

Agarwal, V., Bell, G.W., Nam, J.W., and Bartel, D.P. (2015). Predicting effective microRNA target sites in mammalian mRNAs. eLife *4*, e05005.

Auyeung, V.C., Ulitsky, I., McGeary, S.E., and Bartel, D.P. (2013). Beyond secondary structure: primary-sequence determinants license pri-miRNA hairpins for processing. Cell *152*, 844–858.

Ballarino, M., Pagano, F., Girardi, E., Morlando, M., Cacchiarelli, D., Marchioni, M., Proudfoot, N.J., and Bozzoni, I. (2009). Coupled RNA processing and transcription of intergenic primary microRNAs. Mol. Cell. Biol. *29*, 5632–5638.

Baltz, A.G., Munschauer, M., Schwanhäusser, B., Vasile, A., Murakawa, Y., Schueler, M., Youngs, N., Penfold-Brown, D., Drew, K., Milek, M., et al. (2012). The mRNA-bound proteome and its global occupancy profile on protein-coding transcripts. Mol. Cell *46*, 674–690.

Bartel, D.P. (2009). MicroRNAs: target recognition and regulatory functions. Cell *136*, 215–233.

Burge, R.G., Martinez-Yamout, M.A., Dyson, H.J., and Wright, P.E. (2014). Structural characterization of interactions between the double-stranded RNA-binding zinc finger protein JAZ and nucleic acids. Biochemistry *53*, 1495–1510.

Bushati, N., and Cohen, S.M. (2007). microRNA functions. Annu. Rev. Cell Dev. Biol. *23*, 175–205.

Castello, A., Fischer, B., Eichelbaum, K., Horos, R., Beckmann, B.M., Strein, C., Davey, N.E., Humphreys, D.T., Preiss, T., Steinmetz, L.M., et al. (2012). Insights into RNA biology from an atlas of mammalian mRNA-binding proteins. Cell *149*, 1393–1406.

Chang, H.M., Triboulet, R., Thornton, J.E., and Gregory, R.I. (2013). A role for the Perlman syndrome exonuclease Dis3l2 in the Lin28-let-7 pathway. Nature *497*, 244–248.

Choudhury, N.R., and Michlewski, G. (2012). Terminal loop-mediated control of microRNA biogenesis. Biochem. Soc. Trans. *40*, 789–793.

Choudhury, N.R., de Lima Alves, F., de Andrés-Aguayo, L., Graf, T., Cáceres, J.F., Rappsilber, J., and Michlewski, G. (2013). Tissue-specific control of brain-enriched miR-7 biogenesis. Genes Dev. *27*, 24–38.

Choudhury, N.R., Nowak, J.S., Zuo, J., Rappsilber, J., Spoel, S.H., and Michlewski, G. (2014). Trim25 is an RNA-specific activator of Lin28a/TuT4-mediated uridylation. Cell Rep. *9*, 1265–1272.

Cong, L., Ran, F.A., Cox, D., Lin, S., Barretto, R., Habib, N., Hsu, P.D., Wu, X., Jiang, W., Marraffini, L.A., and Zhang, F. (2013). Multiplex genome engineering using CRISPR/Cas systems. Science *339*, 819–823.

Connerty, P., Ahadi, A., and Hutvagner, G. (2016). RNA binding proteins in the miRNA pathway. Int. J. Mol. Sci. *17*, 31.

Contrant, M., Fender, A., Chane-Woon-Ming, B., Randrianjafy, R., Vivet-Boudou, V., Richer, D., and Pfeffer, S. (2014). Importance of the RNA secondary structure for the relative accumulation of clustered viral microRNAs. Nucleic Acids Res. *42*, 7981–7996.

Cox, J., Hein, M.Y., Luber, C.A., Paron, I., Nagaraj, N., and Mann, M. (2014). Accurate proteome-wide label-free quantification by delayed normalization and maximal peptide ratio extraction, termed MaxLFQ. Mol. Cell. Proteomics *13*, 2513–2526.

Davis, B.N., Hilyard, A.C., Lagna, G., and Hata, A. (2008). SMAD proteins control DROSHA-mediated microRNA maturation. Nature *454*, 56–61.

Du, P., Wang, L., Sliz, P., and Gregory, R.I. (2015). A biogenesis step upstream of microprocessor controls miR-17∼92 expression. Cell *162*, 885–899.

Dueck, A., and Meister, G. (2014). Assembly and function of small RNA - argonaute protein complexes. Biol. Chem. *395*, 611–629.

Edwards, J., Malaurie, E., Kondrashov, A., Long, J., de Moor, C.H., Searle, M.S., and Emsley, J. (2011). Sequence determinants for the tandem recognition of UGU and CUG rich RNA elements by the two N–terminal RRMs of CELF1. Nucleic Acids Res. *39*, 8638–8650.

Faehnle, C.R., Walleshauser, J., and Joshua-Tor, L. (2014). Mechanism of Dis3l2 substrate recognition in the Lin28-let-7 pathway. Nature *514*, 252–256.

Gerstberger, S., Hafner, M., and Tuschl, T. (2014). A census of human RNA-binding proteins. Nat. Rev. Genet. *15*, 829–845.

Good, P.J., Chen, Q., Warner, S.J., and Herring, D.C. (2000). A family of human RNA-binding proteins related to the Drosophila Bruno translational regulator. J. Biol. Chem. *275*, 28583–28592.

Guil, S., and Cáceres, J.F. (2007). The multifunctional RNA-binding protein hnRNP A1 is required for processing of miR-18a. Nat. Struct. Mol. Biol. *14*, 591–596.

Hannus, M., Beitzinger, M., Engelmann, J.C., Weickert, M.T., Spang, R., Hannus, S., and Meister, G. (2014). siPools: highly complex but accurately defined siRNA pools eliminate off-target effects. Nucleic Acids Res. *42*, 8049–8061.

He, L., Thomson, J.M., Hemann, M.T., Hernando-Monge, E., Mu, D., Goodson, S., Powers, S., Cordon-Cardo, C., Lowe, S.W., Hannon, G.J., and Hammond, S.M. (2005). A microRNA polycistron as a potential human oncogene. Nature *435*, 828–833.

He, L., He, X., Lim, L.P., de Stanchina, E., Xuan, Z., Liang, Y., Xue, W., Zender, L., Magnus, J., Ridzon, D., et al. (2007). A microRNA component of the p53 tumour suppressor network. Nature *447*, 1130–1134.

Heo, I., Joo, C., Cho, J., Ha, M., Han, J., and Kim, V.N. (2008). Lin28 mediates the terminal uridylation of let-7 precursor MicroRNA. Mol. Cell *32*, 276–284.

Heo, I., Joo, C., Kim, Y.K., Ha, M., Yoon, M.J., Cho, J., Yeom, K.H., Han, J., and Kim, V.N. (2009). TUT4 in concert with Lin28 suppresses microRNA biogenesis through pre-microRNA uridylation. Cell *138*, 696–708.

Heo, I., Ha, M., Lim, J., Yoon, M.J., Park, J.E., Kwon, S.C., Chang, H., and Kim, V.N. (2012). Mono-uridylation of pre-microRNA as a key step in the biogenesis of group II let-7 microRNAs. Cell *151*, 521–532.

Hurteau, G.J., Spivack, S.D., and Brock, G.J. (2006). Potential mRNA degradation targets of hsa-miR-200c, identified using informatics and qRT-PCR. Cell Cycle *5*, 1951–1956.

Jonas, S., and Izaurralde, E. (2015). Towards a molecular understanding of microRNA-mediated gene silencing. Nat. Rev. Genet. *16*, 421–433.

Kawahara, Y., and Mieda-Sato, A. (2012). TDP-43 promotes microRNA biogenesis as a component of the Drosha and Dicer complexes. Proc. Natl. Acad. Sci. USA *109*, 3347–3352.

Kim, V.N., Han, J., and Siomi, M.C. (2009). Biogenesis of small RNAs in animals. Nat. Rev. Mol. Cell Biol. *10*, 126–139.

Kim, Y.K., Heo, I., and Kim, V.N. (2010). Modifications of small RNAs and their associated proteins. Cell *143*, 703–709.

Lin, S., and Gregory, R.I. (2015). MicroRNA biogenesis pathways in cancer. Nat. Rev. Cancer *15*, 321–333.

Loedige, I., Jakob, L., Treiber, T., Ray, D., Stotz, M., Treiber, N., Hennig, J., Cook, K.B., Morris, Q., Hughes, T.R., et al. (2015). The crystal structure of the NHL domain in complex with RNA reveals the molecular basis of Drosophila brain-tumor-mediated gene regulation. Cell Rep. *13*, 1206–1220.

Michlewski, G., Guil, S., and Cáceres, J.F. (2010). Stimulation of pri-miR-18a processing by hnRNP A1. Adv. Exp. Med. Biol. *700*, 28–35.

Morlando, M., Dini Modigliani, S., Torrelli, G., Rosa, A., Di Carlo, V., Caffarelli, E., and Bozzoni, I. (2012). FUS stimulates microRNA biogenesis by facilitating co-transcriptional Drosha recruitment. EMBO J. *31*, 4502–4510.

Newman, M.A., Thomson, J.M., and Hammond, S.M. (2008). Lin-28 interaction with the Let-7 precursor loop mediates regulated microRNA processing. RNA *14*, 1539–1549.

Oellerich, T., Bremes, V., Neumann, K., Bohnenberger, H., Dittmann, K., Hsiao, H.H., Engelke, M., Schnyder, T., Batista, F.D., Urlaub, H., and Wienands, J. (2011). The B-cell antigen receptor signals through a preformed transducer module of SLP65 and CIN85. EMBO J. *30*, 3620–3634.

Raver-Shapira, N., Marciano, E., Meiri, E., Spector, Y., Rosenfeld, N., Moskovits, N., Bentwich, Z., and Oren, M. (2007). Transcriptional activation of miR-34a contributes to p53-mediated apoptosis. Mol. Cell *26*, 731–743.

Ray, D., Kazan, H., Cook, K.B., Weirauch, M.T., Najafabadi, H.S., Li, X., Gueroussov, S., Albu, M., Zheng, H., Yang, A., et al. (2013). A compendium of RNA-binding motifs for decoding gene regulation. Nature *499*, 172–177.

Rybak, A., Fuchs, H., Smirnova, L., Brandt, C., Pohl, E.E., Nitsch, R., and Wulczyn, F.G. (2008). A feedback loop comprising lin-28 and let-7 controls pre-let-7 maturation during neural stem-cell commitment. Nat. Cell Biol. *10*, 987–993.

Slack, F.J., Basson, M., Liu, Z., Ambros, V., Horvitz, H.R., and Ruvkun, G. (2000). The lin-41 RBCC gene acts in the C. elegans heterochronic pathway between the let-7 regulatory RNA and the LIN-29 transcription factor. Mol. Cell *5*, 659–669.

Tabach, Y., Billi, A.C., Hayes, G.D., Newman, M.A., Zuk, O., Gabel, H., Kamath, R., Yacoby, K., Chapman, B., Garcia, S.M., et al. (2013). Identification of small RNA pathway genes using patterns of phylogenetic conservation and divergence. Nature *493*, 694–698.

Tarasov, V., Jung, P., Verdoodt, B., Lodygin, D., Epanchintsev, A., Menssen, A., Meister, G., and Hermeking, H. (2007). Differential regulation of microRNAs by p53 revealed by massively parallel sequencing: miR-34a is a p53 target that induces apoptosis and G1-arrest. Cell Cycle *6*, 1586–1593.

Thornton, J.E., Du, P., Jing, L., Sjekloca, L., Lin, S., Grossi, E., Sliz, P., Zon, L.I., and Gregory, R.I. (2014). Selective microRNA uridylation by Zcchc6 (TUT7) and Zcchc11 (TUT4). Nucleic Acids Res. *42*, 11777–11791.

Trabucchi, M., Briata, P., Garcia-Mayoral, M., Haase, A.D., Filipowicz, W., Ramos, A., Gherzi, R., and Rosenfeld, M.G. (2009). The RNA-binding protein KSRP promotes the biogenesis of a subset of microRNAs. Nature *459*, 1010–1014.

Treiber, T., Treiber, N., and Meister, G. (2012). Regulation of microRNA biogenesis and function. Thromb. Haemost. *107*, 605–610.

Triboulet, R., Pirouz, M., and Gregory, R.I. (2015). A single Let-7 microRNA bypasses LIN28-mediated repression. Cell Rep. *13*, 260–266.

Viswanathan, S.R., Daley, G.Q., and Gregory, R.I. (2008). Selective blockade of microRNA processing by Lin28. Science *320*, 97–100.

Vizcaíno, J.A., Csordas, A., Del-Toro, N., Dianes, J.A., Griss, J., Lavidas, I., Mayer, G., Perez-Riverol, Y., Reisinger, F., Ternent, T., et al. (2016). 2016 update of the PRIDE database and its related tools. Nucleic Acids Res. *44*, 11033.

Wu, S.L., Fu, X., Huang, J., Jia, T.T., Zong, F.Y., Mu, S.R., Zhu, H., Yan, Y., Qiu, S., Wu, Q., et al. (2015). Genome-wide analysis of YB-1-RNA interactions reveals a novel role of YB-1 in miRNA processing in glioblastoma multiforme. Nucleic Acids Res. *43*, 8516–8528.

Xiong, X.P., Vogler, G., Kurthkoti, K., Samsonova, A., and Zhou, R. (2015). SmD1 modulates the miRNA pathway independently of its pre-mRNA splicing function. PLoS Genet. *11*, e1005475.

Zeng, Y., Yao, B., Shin, J., Lin, L., Kim, N., Song, Q., Liu, S., Su, Y., Guo, J.U., Huang, L., et al. (2016). Lin28A binds active promoters and recruits Tet1 to regulate gene expression. Mol. Cell *61*, 153–160.

Zhou, R., Hotta, I., Denli, A.M., Hong, P., Perrimon, N., and Hannon, G.J. (2008). Comparative analysis of argonaute-dependent small RNA pathways in Drosophila. Mol. Cell *32*, 592–599.

STAR★METHODS

KEY RESOURCES TABLE

REAGENT or RESOURCE	SOURCE	IDENTIFIER
Antibodies		
αHA	Covance	Ha.11, clone 16B12; RRID: AB_2314672
αRBM10	Abcam	ab72423 LOT GR60990-2; RRID:AB_1270200
αLIN28A	Abcam	ab46020 LOT #904781; RRID:AB_776033
αHNRNPA1	Santa Cruz Biotechnology	sc-32301, clone 4B10; RRID:AB_627729
αZNF346	Abcam	ab96198; RRID:AB_10678096
αDDX21	Bethyl	A300-628A, Lot No. A300-628A-1; RRID:AB_513603
αMATR3	Bethyl	A300-591A, Lot No. A300-591A-1; RRID:AB_495514
αTRIM71	gift of G. Wulczyn	
IRDye 800CW Goat anti-Mouse IgG	Li-Cor	926-32210 Lot C50113-06
RDye 800CW Goat anti-Rabbit IgG	Li-Cor	926-32211 Lot C30829-02
Alexa Fluor 488 rabbit-anti-mouse IgG	Life Technologies	A11059 Lot 1348651
Bacterial and Virus Strains		
E. Coli BL21(DE3)	Invitrogen	n/a
E. Coli Rosetta	Novagen	70954-3
Chemicals, Peptides, and Recombinant Proteins		
T7 RNA-Polymerase	our lab	n/a
ZC3H10 (aa. 35-168)	our lab	n/a
truncated T4 RNA Ligase 2	our lab	n/a
PUM1 (aa. 828-1176)	our lab	n/a
T4 RNA Ligase 1	NEB	M0204
Thermostable inorganic pyrophosphatase	NEB	M0296
E. Coli Poly(A) Polymerase	NEB	M0276
Ribolock Ribonuclease Inhibitor	ThermoFisher Scientific	EO0381
TRIzol reagent	ThermoFisher Scientific	15596-018
Sequa Gel	National Diagnostics	EC-833
Magnetic streptavidin beads (M-270)	Invitrogen	65306
ANTI-FLAG M2 Affinity Gel	Sigma Aldrich	A2220
NuPAGE Novex gels (4%–12% Bis-Tris-Gel gradient gels, 1.0 mm)	Thermo Fisher Scientific	NP0321

(*Continued on next page*)

Continued

REAGENT or RESOURCE	SOURCE	IDENTIFIER
NuPAGE LDS Sample Buffer	Thermo Fisher Scientific	NP0008
NuPAGE Sample Reducing Agent	Thermo Fisher Scientific	NP0009
γ^{32}P-ATP	Hartmann Analytic	FP-501
SsoFast EvaGreen Supermix	Biorad	1725204
Prolong Gold Antifade Mountant with DAPI	Life Technologies	P36931
Lipofectamine 2000	Invitrogen	11668500
Lipofectamine RNAiMax	Thermo Fisher Scientific	13778500
EDC (1-ethyl-3-(3-dimethylaminopropyl)-carbodiimide hydrochloride	Sigma Aldrich	E1769
Critical Commercial Assays		
First-strand cDNA synthesis kit	ThermoFisher Scientific	K1612
SuperScriptIII First Strand Synthesis Super Mix	Invitrogen	18080400
MiSeq Reagent Kit V3 (150cycle)	Illumina	MS-102-3001
Deposited Data		
Mass-spectrometry Data of pull-down experiments	ProteomeXchange	PXD004193
Experimental Models: Cell Lines		
human: MCF7	our lab	ATCC® HTB-22
human: DLD-1	ATCC	ATCC® CCL-221
human: LN-229	our lab	ATCC® CRL-2611
human: HEPG2	our lab	ATCC® HB-8065
human: Jurkat	Grosschedl lab, Freiburg	ATCC® TIB-152
human: HEK293T	our lab	ATCC® CRL-3216
human: HeLa	our lab	ATCC® CCL-2
human: A549	ATCC	ATCC® CCL-185
human: SK-MEL-28	ATCC	ATCC® HTB-72
human: SK-N-MC	ATCC	ATCC® HTB-10
human: DU145	ATCC	ATCC® HTB-81
human: Raji	Grosschedl lab, Freiburg	ATCC® CCL-86
human: NTERA-2	ATCC	ATCC® CRL-1973
CRISPR/CAS9-edited cell lines were derived from these cell lines; see Table S6	this study	n/a
Oligonucleotides		
siRNAs (siPools)	SiTools Biotech	n/a
3′-biotinylated 2′-O-methyl-RNA adaptor (5′-AGGCUAG GUCUCCC-3′)	Metabion Eurofins	n/a
primer sequences for strand-specific cDNA-synthesis, see Table S5	Metabion	n/a
primer sequences for pri-miRNA profiling by qPCR see Table S5	Metabion	n/a
Northern blot probe sequences, see Table S5	Metabion	n/a
sequences of oligos used for library preparation, see Table S5	Metabion	n/a
primers for Poly(A)-Tailing and pre-miRNA RT-qPCR, see Table S5	Metabion	n/a
primers for analysis of CRISPR/CAS-generated knockout clones, see Table S5	Metabion	n/a

(*Continued on next page*)

Continued

REAGENT or RESOURCE	SOURCE	IDENTIFIER
RNAs for EMSAs	Metabion	n/a
5′-lower stem: AGCAGCGCA;		
3′-lower stem: AGUUCUGCA.		
2′-O-methyl-RNAs for miRNA inhibitor assay	Metabion	n/a
miRNA-29a inhibitor		
5′-UAACCGAUUUCAGAUGGUGCUA-3′		
scrambled control		
5′-CAUCACGUACGCGGAAUACUU-3		
gene specific qPCR primers, see Table S5	Metabion	n/a
Recombinant DNA		
pGEM-T	Promega	A3600
pGEM-T easy	Promega	A1360
pGEM-T and pGEM-T easy containing sequences for miRNA-hairpins with the 5′-adaptor sequence and mutants, see Table S5	this study	n/a
pX330 vector	Zhang lab	Addgene 42230
pX330 containing gRNA-sequences; see STAR Methods	this study	n/a
pIRES-puro vector	Clontech	631619
VP5	Roeder lab, New York	n/a
VP5-GFP	our lab	n/a
VP5 containing candidate genes; see Table S5	this study	n/a
pSuperior-CMV	our lab	n/a
pSuperior containing sequences for “pri”-miRNA; see Table S5	this study	n/a
pGEX-4T-1	GE Healthcare	28-9545-49
pGEX_ZC3H10$^{35\text{-}168}$	this study	n/a
pColdI	takara bio	3361
pColdI_PUM1$^{828\text{-}1176}$	this study	n/a
Software and Algorithms		
Scaffold	Proteome Software	Version 4.3.2
MaxQuant	http://www.coxdocs.org/doku.php?id=maxquant:start	Cox et al., 2014
Mascot	Matrix Science	Version 2.3.02
UNIPROT knowledgebase	http://www.uniprot.org	
Gene Ontology Consortium	http://geneontology.org	
Ortholist server	http://www.greenwaldlab.org/ortholist	
BioMart tool	http://www.ensembl.org//useast.ensembl.org/biomart?redirectsrc=//www.ensembl.org%2Fbiomart	
Mirbase	http://www.mirbase.org	
Flybase	http://.flybase.org	
NCBI nr database		Accessed 13.09.2011

CONTACT FOR REAGENT AND RESOURCE SHARING

Further information and requests for resources and reagents should be directed to and will be fulfilled by the Lead Contact, Gunter Meister (gunter.meister@vkl.uni-regensburg.de).

EXPERIMENTAL MODEL AND SUBJECT DETAILS

The cells lines used in this study are listed below. Raji and Jurkat cells were grown in RPMI-1640 medium containing 10% FCS and antibiotics. All other cells were grown in DMEM medium with 10% FCS and antibiotics.

Name	Species	Tissue	Sex	Disease	Identifier
MCF7	human	mammary gland, breast	female	adenocarcinoma	ATCC® HTB-22
DLD-1	human	colon	male	colorectal adenocarcinoma	ATCC® CCL-221
LN-229	human	brain	female	glioblastoma	ATCC® CRL-2611
HEPG2	human	liver	male	hepatocellular carci*noma*	ATCC® HB-8065
Jurkat	human	peripheral blood	male	acute t cell leukemia	ATCC® TIB-152
HEK293	human	embryonic kidney	female		ATCC® CRL-3216
HeLa	human	cervix	female	adenocarcinoma	ATCC® CCL-2
A549	human	lung	male	carcinoma	ATCC® CCL-185
SK-MEL-28	human	skin	male	malignant melanoma	ATCC® HTB-72
SK-N-MC	human	brain	female	neuroepithelioma	ATCC® HTB-10
DU145	human	prostate	male	carcinoma	ATCC® HTB-81
Raji	human	lymphoblast	male	burkitt's lymphoma	ATCC® CCL-86
NTERA-2	human	testis	male	malignant pluripotent embryonal carcinoma	ATCC® CRL-1973

CRISPR/Cas9-edited clones of the cell lines were cultured as the parental cell line. For the genotypes of the edited alleles, see Table S6.

METHOD DETAILS

Pri-miRNA Screening by qPCR

For each of the investigated cell lines, three independent biological samples were harvested by trypsination and RNA was extracted using *TRIzol* reagent (Invitrogen). cDNA was synthesized using the *First-strand cDNA synthesis kit* (Thermo Fisher Scientific) with random hexameric primers. For miRNAs encoded in antisense orientation to mRNA transcripts (pri-miR-1-2, pri-miR-199a-1, pri-miR-199a-2 and pri-miR-214) and for U1 snRNA as a control, strand-specific cDNA-synthesis was performed using a mix of gene-specific primers as listed in Table S5.

Primers efficiencies for pri-miRNA profiling were tested using genomic DNA from HEK293 cells in order to allow comparison of absolute miRNA levels between different primer pairs. In addition, only primer pairs were accepted that showed consistent linear amplification differences over a dilution series of DNA. The resulting primers used for profiling are listed in Table S5. For qPCR-profiling, 2% of a cDNA-synthesis reaction from 2 μg of total RNA was used in a 20 μl reaction using *SsoFast EvaGreen Supermix* (Biorad) and 0.25 μmol of each primer. The results were normalized against U1 snRNA and corrected for their different primer efficiencies. The values for the biological triplicates were averaged and standard deviations were calculated. All standard deviations were below 1 cycle.

Profiling of microRNAs by Northern Blot

Total RNA was extracted from cell samples using *TRIzol* reagent (Invitrogen). 20 μg RNA of each cell line was loaded on a 12% urea acrylamide gel (*Sequa Gel*, National diagnostics) and run at 350 V with TBE as running buffer. Integrity of the RNA was checked by ethidium bromide staining. The nucleid acid was then transferred onto a nylon membrane (*Hybond-N*, GE Healthcare) by semi-dry blotting (20 V, 1 h) and crosslinked with EDC (1-ethyl-3-(3-dimethylaminopropyl)-carbodiimide hydrochloride) and 1-methylimidazole for 1 hr at 50°C. The membranes were hybridized with ^{32}P-labeled probes overnight at 50°-65°C (refer to Table S5 for probe sequences and hybridization conditions) in a hybridization solution containing 5x SSC, 7% (w/v) SDS, 20 mM sodium phosphate buffer, pH 7, and 2% Denhardt's solution. The blots were washed twice with a solution containing 5x SSC and 1% (w/v) SDS and once with a solution of 1x SSC and 1% (w/v) SDS at the respective hybridization temperature. The radioactive signals were analyzed using storage screens and a PMI system (Biorad).

For detection of specific miRNAs, RNA-probes were developed that not only recognize the mature miRNA but also the loop sequence. These probes are more sensitive to pre-miRNAs and therefore could in some cases detect that low abundant intermediate product. RNA-probes were produced by *in-vitro* transcription as described below. For U6 snRNA and AT-rich miRNA sequences DNA-probes complementary to the mature sequence were used (Table S5).

After exposure, the probes were stripped of the membranes using hot 0.1% SDS solution. An overnight exposure was performed to ensure total loss of the hybridization signal. Stripped membranes were reprobed with control- or additional miRNA-probes.

Profiling of Mature miRNAs by Deep Sequencing

1 μg of total RNA was ligated to a previously adenylated 3′-adaptor by a truncated T4 RNA Ligase 2. In a second ligation step a 5′ RNA adaptor was added by T4 RNA Ligase 1. The product was reverse-transcribed using the *SuperScriptIII First Strand Synthesis Super Mix* (Invitrogen) and a specific primer (RT-primer), followed by a PCR amplification, with the 3′ primer containing a 6 nt barcode. The samples were run on a 6% Urea-PA-Gel (National Diagnostics), the bands corresponding to small RNA containing ligation products were cut out and eluted overnight in 300 mM NaCl, 2 mM EDTA. The libraries were precipitated with ethanol overnight at −20°C, then collected by centrifugation and dissolved in water. All oligos used for library preparation are listed in Table S5.

Generation of hairpin baits for RBP-Pull-down

For production of fragments of pri-miRNA baits the desired sequences were first amplified from genomic DNA and cloned into pGEM-T (Invitrogen). The sequences of obtained plasmids were verified by Sanger-sequencing. The constructs contain a T7-promotor (marked in bold) followed by a 5′-extension (marked in red) and are listed in Table S5, with the mature sequences highlighted in dark green and the star strand colored in light green.

For in vitro transcription, the template sequences were first amplified by PCR using the sequence-verified plasmid template. 2 μg of the PCR-product was then used in a 1 mL transcription reaction containing 30 mM Tris, pH 8.0, 10 mM DTT, 0.01% Triton X-100, 25 mM $MgCl_2$, 2 mM spermidine, 5 mM ADP, 5 mM CTP, 5 mM UTP, 5 mM GTP, 0.4 U/ml thermostable inorganic pyrophosphatase (NEB) and 0.1 mg/ml T7-polymerase at 37°C for at least 4 hr. RNA-products were separated by urea-PAGE. RNA-bands were visualized by UV shadowing, cut out and eluted with water. NaCl was added to 500 mM f.c. and the RNA precipitated with 0.7 volumes of 2-propanol, washed with 80% (v/v) ethanol and air-dried.

Pull-down of miRNA hairpin-binding Proteins

For each pull-down sample 100 μl of magnetic streptavidin beads (M-270, Invitrogen) were washed with lysis buffer (50 mM Tris, pH 8.0, 150 mM NaCl, 5% (v/v) glycerol, 1 mM DTT, 1 mM AEBSF) and coupled to 4 μg of a 3′-biotinylated 2′-O-methyl-RNA adaptor (5′-AGGCUAGGUCUCCC-3′) for 1 hr at 4°C in 500 μl lysis buffer. After two washing steps with lysis buffer, half of the adaptor-coupled beads were removed and stored at 4°C for preclearing. The second half was incubated with 10 μg of the bait RNA hairpin in 500 μl lysis buffer overnight at 4°C and washed twice with lysis buffer directly before adding the cell lysate.

For the preparation of cell lysate, two 15 cm-plates of confluent cells were harvested, resuspended in 1 mL lysis buffer and lysed by sonication. Insoluble matter was removed by centrifugation (30 min, 20000 g, 4°C) and the supernatant subjected to a preclearing step by adding the adaptor-coupled beads and rotating for 3-4 hr at 4°C. After removal of the beads, the supernatant was used for the pull-down experiment.

To capture binders of the miRNA-baits, the RNA-coupled beads were incubated with the precleared lysate at 4°C overnight while rotating. The beads were then washed successively with 1 mL of washbuffer I (lysis buffer containing 300 mM NaCl), 1 mL of wash-buffer II (lysis buffer supplemented with 0.1% (v/v) Triton X-100) and 1 mL lysis buffer. Beads were resuspended in 35 μl loading dye (*NuPAGE LDS Sample Buffer with NuPAGE Sample Reducing Agent* (Thermo Fisher Scientific)).

Mass Spectrometry Analysis

Affinity purified samples were separated on NuPAGE gels (4 – 12% Bis-Tris-Gel gradient gels, 1.0 mm) according to the manufacturer's protocol. Samples were run until the front reached half of the gel. The gels were Coomassie stained and each sample was cut into twelve slices and proteins in the gel slices were digested with endoproteinase trypsin under standard conditions. Peptides were extracted and subjected to LC-MS analyses on an Orbitrap XL mass spectrometer (ThermoFisherScientific) coupled to an Agilent 1100 Series liquid chromatography system exactly as described in (Oellerich et al., 2011) except that peptides were separated with a linear gradient of 3% (v/v) solvent B to 36% (v/v) solvent B in 90 min. Solvent A was 0.1% (v/v) formic acid (FA) in water and solvent B was 95% (v/v) acetonitrile (ACN), 0.1% (v/v) FA in water. MS raw data were searched using Mascot (MatrixScience, version 2.3.02) as search engine against NCBInr database (13.09.2011, taxonomy human with 229340

entries) with the following parameters: two missed cleavages allowed, MS1 mass deviation 10 ppm, MS2 mass deviation 0.6 Da, variable modifications: Oxidation of Met, carbamidomethylation of Cys. Data were evaluated using Scaffold 4.3.2. (Proteome Software).

Analysis of Mass Spectrometry Data

For the analysis of the bound proteins from the pull-down screen, all identified proteins from the eleven cell lines were sorted according to their NCBI accession code. Different isoforms of the same protein were handled as one hit. Each identified protein was manually analyzed for specific binding to one or a subset of the 72 miRNA baits according to the unweighted spectrum counts. Unweighted spectrum counts of 1 were omitted. Only proteins whose binding specificity was consistent throughout all the cell lines, in which it could be identified, were considered as specific binders. Proteins which were only identified in one cell line were not accounted for, as they lacked a consistency control. They are, however, listed in Table S2. As an exception of this, proteins identified in a single cell line were included when they were also part of a larger complex of which a different subunit had already been identified as a candidate binder. During the assessment of the data the previously annotated function of the identified proteins was disregarded. However, we omitted the mitochondrial ribosome, several subunits of which were found bound to pri-miRNA-34b, from the final heatmap for better readability.

Throughout our analyses, we used the unweighted spectrum counts from the Scaffold evaluation. To confirm that this approach is valid, we analyzed a number of randomly selected datasets by label free quantification (LFQ) using MaxQuant (Cox et al., 2014) and observed a good correlation between LFQ scores and spectrum counts (data not shown). Due to the already massive amount of instrument time, we did not perform a mass spec analysis of the input. Instead, we defined the sum of spectrum counts for a protein measured with all 72 miRNA bait samples in one cell line as the "total spectrum count" of that protein in the given cell line and used this number for normalization.

Neither the pull-down assay nor the mass spectrometry analysis of the bound proteins are quantitative – however, to better visualize the specificity of the identified miRNA-binders, we calculated two heatmaps: For the first heatmap, the percentage of the spectrum count for a candidate protein bound to each miRNA bait relative to the total spectrum count of that protein found in a given cell line (as defined above) was calculated. The resulting percentage values were then averaged over all cell lines in which the protein had been identified. However, this heatmap leads to the call of a hit if a weakly identified protein shows a spurious binding event which is not consistent throughout all cell lines. For the second heatmap, we first summarized the unweighted spectrum counts of each miRNA bait for a candidate protein over all cell lines in which that protein was identified. We then normalized these values to the sum of total spectrum counts of that protein from all cell lines, in which it was identified. The disadvantage of this heatmap is the overweighting of cell lines in which a candidate protein is identified in higher amounts, often leading to more background binding. To account for both problems, we averaged both heatmaps for an optimal representation of our binding data. However, to appraise weak hits, it is advisable to always check the original data in Table S2, which also contains more information regarding cell lines and the overall level of the proteins identified.

Data base analysis of candidate proteins

Annotations of known RNA-binding activity and subcellular localization were gathered from the UNIPROT knowledgebase (http://www.uniprot.org). Analysis of enriched GO-terms was performed using the web interface of the Gene Ontology Consortium (http://geneontology.org).

For comparison of the miRNA hairpin binding candidates with genes previously identified as putative small RNA pathway components in the model organisms *C. elegans* and *D. melanogaster*, lists of candidate genes were extracted from the supplemental material of the publications by (Tabach et al., 2013; Zhou et al., 2008). To identify human orthologs of the *C. elegans* dataset, the Ortholist server (http://www.greenwaldlab.org/ortholist) was used and the result transformed into gene symbols using the BioMart tool (http://www.ensembl.org//useast.ensembl.org/biomart?redirectsrc=//www.ensembl.org%2Fbiomart). The *Drosophila* gene set from Zhou et al. (2008) was converted into Flybase gene IDs via the Flybase website (http://.flybase.org) and human orthologs were assigned by BioMart. In both cases multiple human homologs per gene candidate were accepted.

Verification and Analysis of Binding Events

To verify the binding events identified in our large scale screen, we cloned the full length coding sequence for a number of candidate proteins into a mammalian expression vector with a Flag-HA-tag for identification and a CMV promotor for high expression (Table S5). For pull-down experiments the plasmids were transfected into HEK293 cells by the calcium-phosphate method and cells were grown for 1.5-2 days after transfection. Per RNA bait, cells grown from half a 15 cm-plate were used. Pull-down experiments were conducted as described above, but only 50 μl of magnetic beads were coupled to the adaptor, and of these, 20 μl were used for the preclearing procedure and 30 μl for the pull-down experiment.

For verification of the specific binding using endogenous LIN28A protein, two 15 cm plates of confluently grown NTERA-2 cells were harvested for each miRNA bait. The same was done to compare the binding of MATR3 to mir-138-2 or the mir-138-2 mutant. For all other candidates for which the binding was confirmed for the endogenous protein, about $1.5x10^8$ Jurkat cells per miRNA hairpin were used. The pull-down experiment was executed as described for the large-scale screen.

To identify the region of the miRNA haipin that is bound by candidate proteins we cloned chimeric miRNAs hairpins containing the stem of the target miRNA and the loop of an unrelated miRNA and vice versa. The sequences of the chimeric RNA-templates were verified by Sanger sequencing and can be found in Table S5. The chimeric RNA baits were produced as described above and used to pull down HA-tagged candidate proteins from HEK239 cells along with the two parental miRNA hairpins.

Truncations and mutations of mir-143 and mir-9-3 as well as mir-29b-2, mir-138-2, mir-7-1 and mir-140 were also cloned (Table S5) and used in pull-down experiments. Numbering of mutations in the miRNA hairpin refers to the first base of the mature 5p-strand as 1. Mutations are highlighted in pink, and the unchanged loop-parts of truncated hairpins are colored in light blue.

Western Blotting

For detection of proteins by immunoblotting, proteins were first separated on a 10% (w/v) polyacrylamide-SDS-gel (200 V, 2-3 h). Proteins were then transferred onto a nitrocellulose membrane (GE healthcare) using semidry-blotting (20 V, 1.5 h). The membrane was blocked with 5% (w/v) milk powder in TBST 1 hr at room temperature or at 4°C overnight and then decorated with the primary antibody as indicated below. The membrane was washed three times with TBST before adding the cognate secondary antibody (1:10,000 in 5% (w/v) milk powder in TBST) as listed below for 1 hr at room temperature. After washing three times with TBST, the fluorescent label was analyzed using the Li-Cor Odyssey imaging system.

Primary Antibody		Dilution	Source Organism	Incubation Time//Temp	Secondary Antibody (LI-COR)
αHA	Covance (Ha.11, Clone 16B12)	1:1000	mouse, m.c.	1hr // RT	IRDye® 800CW Goat anti-Mouse IgG
αRBM10	Abcam (ab72423)	1:2000	rabbit, p.c.	1hr // RT	IRDye® 800CW Goat anti-Rabbit IgG
αLIN28A	Abcam (ab46020)	1:1000	rabbit, p.c.	1hr // RT	IRDye® 800CW Goat anti-Rabbit IgG
αHNRNPA1	Santa Cruz (sc-32301)	1:1000	mouse, m.c.	1hr // RT	IRDye® 800CW Goat anti-Mouse IgG
αZNF346	Abcam (ab96198)	1:1000	rabbit, p.c.	o/n // 4°C	IRDye® 800CW Goat anti-Rabbit IgG
αDDX21	Bethyl (A300-628A)	1:2000	rabbit, p.c.	o/n // 4°C	IRDye® 800CW Goat anti-Rabbit IgG
αMATR3	Bethyl (A300-591A)	1:5000	rabbit, p.c.	o/n // 4°C	IRDye® 800CW Goat anti-Rabbit IgG
αTRIM71	gift of G. Wulczyn	1:10	mouse, m.c.	o/n // 4°C	IRDye® 800CW Goat anti-Mouse IgG

RNA Immunoprecipitation (RIP)

To analyze the binding of a candidate protein to a miRNA fragment, we performed RNA immunoprecipitation experiments. For analysis by Northern blotting, two 15 cm plates of HEK293 cells were transfected with a plasmid coding for a 300 bp fragment of the pri-miRNA, a control pri-miRNA and the plasmid coding for the flag-HA-tagged protein candidate (1:1:2 mixture). For analysis by RT-qPCR, only one 15 cm plate of HEK293 cells was used. The sequences of the pri-miRNA fragments as well as details for candidate protein overexpression constructs are given in Table S5.

36 hr after transfection, cells were harvested and resuspended in 1 mL lysis buffer containing 25 mM Tris HCl pH 7.5, 150 mM NaCl, 0.5% (v/v) NP-40, 1 mM AEBSF and 1 mM DTT and lysed by incubation on ice for 30 min. After centrifugation (30 min, 20000 g, 4°C), 5% of the lysate was taken as input sample for western blot analysis. Another 5% of the input was used as the input control for Northern Blot or RT-qPCR analysis. For RNA extraction, 1 mL *TRIzol* was added, and RNA was purified as described by the manufacturer. For the precipitation, 20 μg glycogen (ThermoFisher Scientific) were added. The rest of the lysate was used for the pull-down experiment.

For each pull-down experiment, 20 μL of ANTI-FLAG M2 Affinity Gel (Sigma Aldrich) were washed twice with lysis buffer before adding it to the lysate. The pull-down was performed for 2-3 hr at 4°C while rotating. Beads were washed four times with wash buffer containing 25 mM Tris HCl pH 7.5, 150 mM NaCl, 0.05% (v/v) NP-40, 1 mM AEBSF and 1 mM DTT. During the last washing step, the beads were transferred to a fresh reaction tube. Beads were resuspended in 500 μL wash buffer and 10% were used as western blot

sample. The remaining beads were spun down again. For qRT-PCR analysis, RNA was extracted with TRIzol as described above. For Northern blot analysis, beads were resuspended in 200 μl Proteinase K Buffer (300 mM NaCl, 200 mM Tris-HCl, pH7.5, 25 mM EDTA, 2% (w/v) SDS) with 40 μg of proteinase K and incubated for 30 min at 50°C while shaking gently (300 rpm). RNA was prepared by phenol-chloroform extraction and ethanol precipitation.

Poly-A-Tailing and RT- qPCR analysis

To analyze the RNA bound to candidate proteins in a RIP experiment by qPCR, we used a method adapted from (Hurteau et al., 2006) RNA from the RIP experiment was resuspended in 10 μL DEPC-treated water and employed in a 20 μL reaction for Poly-A-Tailing using the *E. Coli* Poly-A Polymerase (NEB) according to the manufacturer's instructions.

10 μL of this reaction was further used for cDNA synthesis using the *First-strand cDNA synthesis kit* (Thermo Fisher Scientific) with a primer (URT-RT) annealing to the beginning of the poly-A-Tail and introducing an annealing site for a subsequent qPCR primer (URT-qPCR). 0.5% were used for qRT-PCR analysis using *SsoFastTM EvaGreen Supermix* (Biorad) and 0.25 μmol of each primer. qPCR was performed using a miRNA-specific primer and a universal reverse primer annealing to the reverse transcriptase priming site (URT-qPCR). The sequences of all primers are listed in Table S5.

Genome Editing Using CRISPR/Cas9

For editing of the genomic loci of the candidate proteins, two gRNAs for each gene were cloned into the pX330 vector from the Zhang lab (Cong et al., 2013) according to their instructions. As the pX330 vector does not confer any antibiotic resistance, we co-transfected the pX330-gRNA-plasmids with an empty pIRES-puro vector (Clontech) to allow for puromycin selection. Furthermore, VP5-GFP was also co-transfected to check for transfection efficiencies. One day after transfection with *Lipofectamine 2000* (Invitrogen), cells were selected for uptake of the plasmid by adding puromycin to the medium for 16 hr. The used puromycin concentrations are listed in below.

Cell Lines	Puromycin Concentration
HEK293	without selection
SK-N-MC	2 μg/ml
NTERA-2	6 μg/ml

After the puromycin-selection, cells were allowed to recover for 2-3 days and then singularized into 96-well plates. For HEK and NTERA-2, 100 cells were used for one 96-well plate. For SK-N-MC, however, 300-500 cells were plated in one 96-well plate, as the cells exhibited a poor rate of clonal outgrowth.

Analysis of Clones from CRISPR/CAS9 editing

To analyze if gene editing by CRISPR/CAS9 had been successful, a PCR-amplicon of about 150 bp containing the gRNA-complementary site was designed for each gRNA used. Primers are given in Table S5 with the common 5′-extension noted in the first line. For preparation of genomic DNA from clonal cell lines, cells were resuspended in 500 μl proteinase K buffer (300 mM NaCl, 200 mM Tris-HCl, pH7.5, 25 mM EDTA, 2% (w/v) SDS) containing 0.2 mg/ml proteinase K and incubated at 50°C overnight. DNA was precipitated by adding 400 μl 2-propanol and centrifugation for 30 min at 21,000 g and 4°C. The pellet was washed with 70% (v/v) ethanol, dried for 5-10 min at 55°C and resuspended in 50 μl water. 3 μl of the DNA-preparation was analyzed in a 50 μl PCR reaction containing 500 nM of each specific primer, 2 μl DMSO, 0.2 mM of each dNTP, 1 U Phusion polymerase and 1x *HF-buffer* (NEB). The reaction protocol consisted of an initial denaturation step at 98°C for 30'', followed by 30 cycles with a 10'' denaturation step at 98°C, a 30'' annealing step at the temperatures given in Table S5 and an elongation step at 72°C for 10''. The reaction was ended with a final elongation step at 72°C for 3 min. PCR-products were analyzed on a 2% (w/v) agarose gel and visualized with *Serva DNA stain G* (Serva). PCR bands were cut out and purified using the *NucleoSpin Gel and PCR Clean-up Kit* (Macherey-Nagel). The PCR products were then subjected to a second round of PCR using barcoded primers from the *TrueSeq-System* (Illumina), gel purified and analyzed on a MiSeq-sequencing platform. The genotypes of the clones used in this study are given in Table S6.

Gene Knockdown by siRNA Pools

Transient knockdown of candidate genes was achieved by transfection of complex pools of siRNAs (siPools, SiTools Biotech). For transfection of one well of a six-well plate, 500 μl GIBCO Opti-MEM were incubated for 10 min with 60 pmol siPool and 5 μl Lipofectamine RNAiMax (Thermo Fisher Scientific). Approximately 200,000 cells in 2.5 mL antibiotic-free DMEM-medium were added, gently mixed and incubated at 37°C, 5% CO2 for 3-4 days. For analysis of miRNA processing, total RNA was extracted using 1 mL *TRIZzol* per well. miRNA-levels were assayed by Northern blotting as described above.

Processing Assay of pri-miRNAs in KO Lines

In view of the fact that primary transcripts of some miRNAs were not present in the HEK-knockout clones of their respective candidate binder, processing activity was monitored using overexpressed primary transcripts. To this end, the sequence of the pre-miRNA flanked by 100nt up- and downstream-sequence was cloned into a vector containing a CMV-promotor. HEK293 cells as well as the knockout clones created by the CRISPR/CAS9 method in HEK were transfected by *Lipofectamin2000* (Invitrogen) with the plasmid for the miRNA of interest as well as an unrelated pri-miRNA as internal control. For this, about 500,000 cells per well were seeded in a six-well plate and cultivated overnight. For transfection, 2.5 μg plasmid DNA (assay pri-miR and control in equal amounts) were used. Experiments were done in triplicates. After 24 hr, cells were harvested by directly adding 1 mL *TRIzol* to each well. RNA-extraction was carried out as described before. Analysis of pre- and mature miRNA-levels was done by Northern Blotting as described above.

Mapping of ZC3H10:pri-miRNA-143 interaction

To find out, which part of ZC3H10 is responsible for the interaction with pri-miR-143, stop codons were introduced into the full length sequence of a plasmid coding for HA-tagged ZC3H10 resulting in two truncations: HA-ZC3H10 (1-168) harbors the three N-terminal C3H1-type zinc-finger motifs, while HA-ZC3H10 (1-288) additionally contains a coiled-coil region located at amino acids 234-280. Furthermore, each of the three zinc finger motifs was destroyed individually and in any combination by introducing point mutations changing the second and third ZN^{2+}-chelating cysteine to serine. All mutants and truncated proteins were produced in HEK293 cells by transfection of the cells with the corresponding plasmids by the calcium phosphate method. Cells were grown for 1.5-2 days after transfection, harvested and used for pull-down assays with mir-143 hairpins as described above.

Purification of recombinant ZC3H10

The zinc finger domain of ZC3H10 (aa. 35-168) was expressed as GST-fusion protein from a pGEX4T1 vector containing an additional TEV-site in front of the ZC3H10 coding sequence. *E. Coli* BL21 transformed with the vector were grown to an OD_{600} of 0.6 and induced with 1 mM IPTG. The induced culture was grown over night at 25°C. The bacteria were lysed by sonication in PBS buffer supplemented with 1M NaCl and 2 mM DTT. The lysate was cleared by centrifugation (50000 g, 35 min, 4°C) and subsequent filtration of the supernatant through a 0.45μm filter membrane (Roth). For capture of the GST-fusion protein, the lysate was run over a 5 mL GSTrap column (GE Healthcare). After extensive washing with lysis buffer, the protein was eluted with 10 mM Glutathion in PBS plus 50 mM Tris pH 8. 0.1 mg/ml TEV protease was added to the pooled protein containing fractions which were subsequently dialyzed over night against a buffer of 100 mM NaCl, 2 mM DTT, 50 mM Tris pH 7.5. The dialyzed fractions were loaded on a Resource Q column (GE Healthcare) preequilibrated with dialysis buffer and the flowthrough containing the ZC3H10 protein was collected. The solution was concentrated to 2 ml total volume using a Vivaspin 20 ultrafiltration device (MWCO 10000, Sartorius) and loaded on a HiLoad 16/60 Superdex S75 gel filtration column (GE Healthcare) equilibrated in 50 mM HEPES pH 7.5, 200 mM NaCl and 1 mM DTT. The peak fractions containing ZC3H10 protein were pooled, concentrated to 2 mg/ml and adjusted to 50% (v/v) glycerol. Aliquots were stored at −80°C.

Electrophoretic Mobility Shift Assay (EMSA)

20 pmol of RNA were 5′ end labeled using Polynucleotide Kinase (Thermo) and γ^{32}P-ATP (Hartmann Analytic). After 1 hr the labeling reaction was stopped by addition of 18 mM EDTA and the labeled RNA was purified with Illustra MicroSpin G25 columns (GE Healthcare). Used oligonucleotides were obtained from Metabion (Munich) and contain a 7-mer motif from the lower stem of the miR-143 flanked by two adenine residues: 5′-lower stem: AGCAGCGCA; 3′lower stem: AGUUCUGCA.

10000 cpm labeled RNA were combined with 0.1 – 3 μM purified ZC3H10 (aa. 35-168) in a 20 μl reaction containing 10mM MOPS pH 7, 50mM KCl, 5mM MgCl2, 5% glycerol, 30 μg/ml heparin and 1 μg yeast t-RNA. The binding reactions were incubated for 10 min at 4°C and separated on a 6% PA-Gel cast in a buffer of 45 mM Tris 45 mM Borate and 5% glycerol. The gel was run at 200 V for 1-2 hr, then dried and exposed to a phosphoimager screen.

miRNA-Inhibitor Assay

400,000 NTERA-2 cells were seeded per well of a 12-well plate and cultured overnight. On the next day the medium was replaced with 1 mL fresh DMEM without antibiotics and the cells were transfected with 100 pmol of 2′O-metyhl RNA using 8 μl Lipofectamine 2000 (Invitrogen). On the following day the cells were split on 6-well plates and grown for 2 additional days before harvesting in 1 mL *TRIzol* reagent (Invitrogen) per well for RNA preparation.

For inhibition of miR-29a an antisense 2′O-methyl RNA was used (5′-UAACCGAUUUCAGAUGGUGCUA-3′), the scrambled control has the sequence 5′-CAUCACGUACGCGGAAUACUU-3′.

Purification of recombinant PUM1 protein

His-tagged PUM1 (aa. 828-1176) was expressed from a pCold1 vector (Takara Bioscience) in the *E. Coli* strain Rosetta. The bacteria were grown to an OD600 of 0.4 at 37°C, then shifted to 15°C and 30 min later induced by addition of 1mM IPTG. After overnight culture at 15°C the culture was harvested and the bacteria were lysed by sonication in 50 mM Na-Phosphate buffer pH 8, with 1 M NaCl and 10 mM Imidazol. The lysate was cleared (50000 g, 35 min 4°C) and filtered before application to a Ni-charged IMAC-Sepharose column (GE Healthcare) preequilibrated in lysis buffer. The protein was eluted using a buffer of 50 mM Na-Phosphate pH 8, 300 mM

NaCl and 500 mM Imidazol. The protein containing fractions were pooled, concentrated to 3 mL total volume using an ultrafiltration device (Vivaspin 20, 10000 MWCO, Sartorius) and applied on a HiLoad Superdex S200 gel filtration column (GE Healthcare). Peak fractions containing His-PUM1 Protein were pooled, concentrated to 7 mg/ml and adjusted to 50% (v/v) Glycerol. Aliquots were stored at −80°C.

Filter Binding Assay

10000 cpm of 32P-labeled pre-miR-199a-1 or pre-miR-145 were diluted in 30μl binding buffer (50 mM Tris-HCl pH 8.0, 150 mM NaCl, 5% glycerol) and incubated with different concentrations of purified PUM1 RNA-binding domain (aa. 828-1176) ranging from 0 to 0.5 μg/μl. After 5′ at 20°C the samples were filtered through a Protran 0.45 nitrocellulose membrane (GE Healthcare) preequilibrated with binding buffer. The membrane was washed once with 20 mL of binding buffer and dried briefly. The spots corresponding to filtered samples were excised and analyzed by scintillation counting. A separate reaction containing the same amount of RNA without protein was not applied to the filter but directly measured by scintillation as total input.

qRT-PCR Analysis of Specific mRNAs

For qRT-PCR analysis of candidate or target mRNAs, cDNA was synthesized using the *First-strand cDNA synthesis kit* (Thermo Fisher Scientific) with random hexameric primers. For qPCR-profiling, 2% of a cDNA-synthesis reaction from 2 μg of total RNA was used in a 20 μl reaction using *SsoFast™ EvaGreen Supermix* (Biorad) and 0.25 μmol of each primer (listed in Table S5). The results were normalized against U1 snRNA.

Immunofluorescence

HeLa cells transfected with HA-tagged overexpression constructs (see Table S5) for candidate proteins were seeded on coverslips 24h post transfection. On the following day, the cells were washed once with PBS and subsequently fixed with 4% Paraformaldehyde in PBS for 10 min at room temperature. To stop the fixation, the paraformaldehyde solution was removed and replaced with a solution of 100 mM glycin in PBS for 5 min. The samples were washed twice with PBS and permeabilized with a solution of 0.2% (v/v) Triton X-100, 3% (w/v) bovine albumin in PBS (15 min, 20°C). Next, the cells were washed with IF-buffer (0.05% (v/v) Triton X-100 and 1% (w/v) bovine albumin in PBS) and incubated in this solution for 1h. A monoclonal antibody against the HA-tag (Covance, 1:200) was applied to the cells for 1h in IF-buffer followed by four washes with this buffer. As secondary antibody, Alexa Fluor 488 rabbit-anti-mouse IgG (Life Technologies) was diluted 1:400 in IF-buffer and incubated for 1h with the samples. After subsequent washes with IF-buffer twice, PBS and water, the coverslips were mounted on microscope slides using Prolong Gold Antifade Mountant with DAPI (Life Technologies) and imaged on a Zeiss Axiovert200M microscope.

QUANTIFICATION AND STATISTICAL ANALYSIS

Northern blot signals were quantified using the Quantity One analysis software Version 4.6.9 (BioRad laboratories) with local background correction. Standard deviations were calculated with Excel.

DATA AND SOFTWARE AVAILABILITY

The mass spectrometry proteomics data have been deposited to the ProteomeXchange Consortium via the PRIDE (Vizcaíno et al., 2016) partner repository with the dataset identifier PRIDE: PXD004193.

Molecular Cell, Volume *66*

Supplemental Information

A Compendium of RNA-Binding Proteins that Regulate MicroRNA Biogenesis

Thomas Treiber, Nora Treiber, Uwe Plessmann, Simone Harlander, Julia-Lisa Daiß, Norbert Eichner, Gerhard Lehmann, Kevin Schall, Henning Urlaub, and Gunter Meister

INDEX

Supplemental Figures and Tables

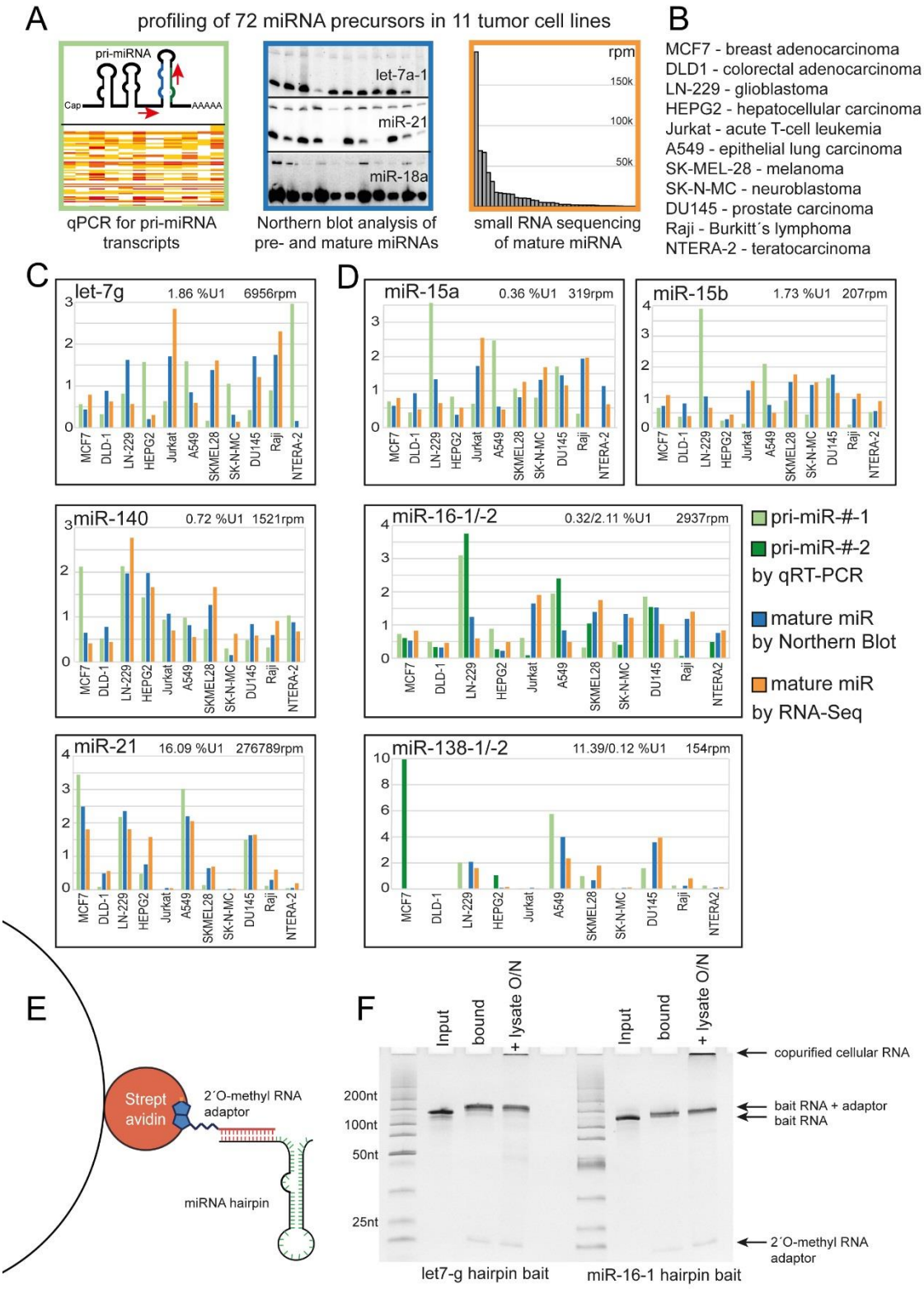

Figure S1 – related to Figure 1: for legend see next page

Figure S1 (previous page) – related to Figure 1

A) Schematic representation of the three approaches used to quantify miRNAs and intermediates of miRNA biogenesis.
B) List of tumor cell lines used for the profiling of miRNA processing and subsequently for pull-down of specific miRNA hairpin binding proteins. Cell line abbreviations and the corresponding tumor type are given.
C), D) Comparative profiles of miRNA processing in the 11 tumor cell lines indicated. Pri-miRNA levels measured by qRT-PCR (green bars), mature miRNA levels measured by northern blot (blue bars) and next generation sequencing (orange bars) are plotted relative to the mean intensity of each data set. If two primary transcripts generate an identical mature miRNA sequence, these are shown in light and dark green, respectively. The mean values for pri-miRNA (expressed as % of U1 snRNA) and mature miRNA (as reads per million) are given in each panel.
E) Schematic representation of the setup used for the pull-down experiments.
F) Analysis of bait stability during the pull-down experiment. 2µg of bait RNA are loaded as input control, bait RNA was eluted from the beads after the coupling step or after overnight incubation with cell lysate from MCF7 cells (1 ml, 8 mg/ml total protein). RNAs were analyzed by Urea-PAGE followed by ethidium bromide staining.

Figure S2 (next page): related to Figure 2

Immunofluorescence staining of pri-miRNA hairpin binding candidate proteins expressed as HA fusion proteins in HeLa-cells. Staining from an anti-HA antibody is shown in the green channel, DNA staining with DAPI is shown in blue.

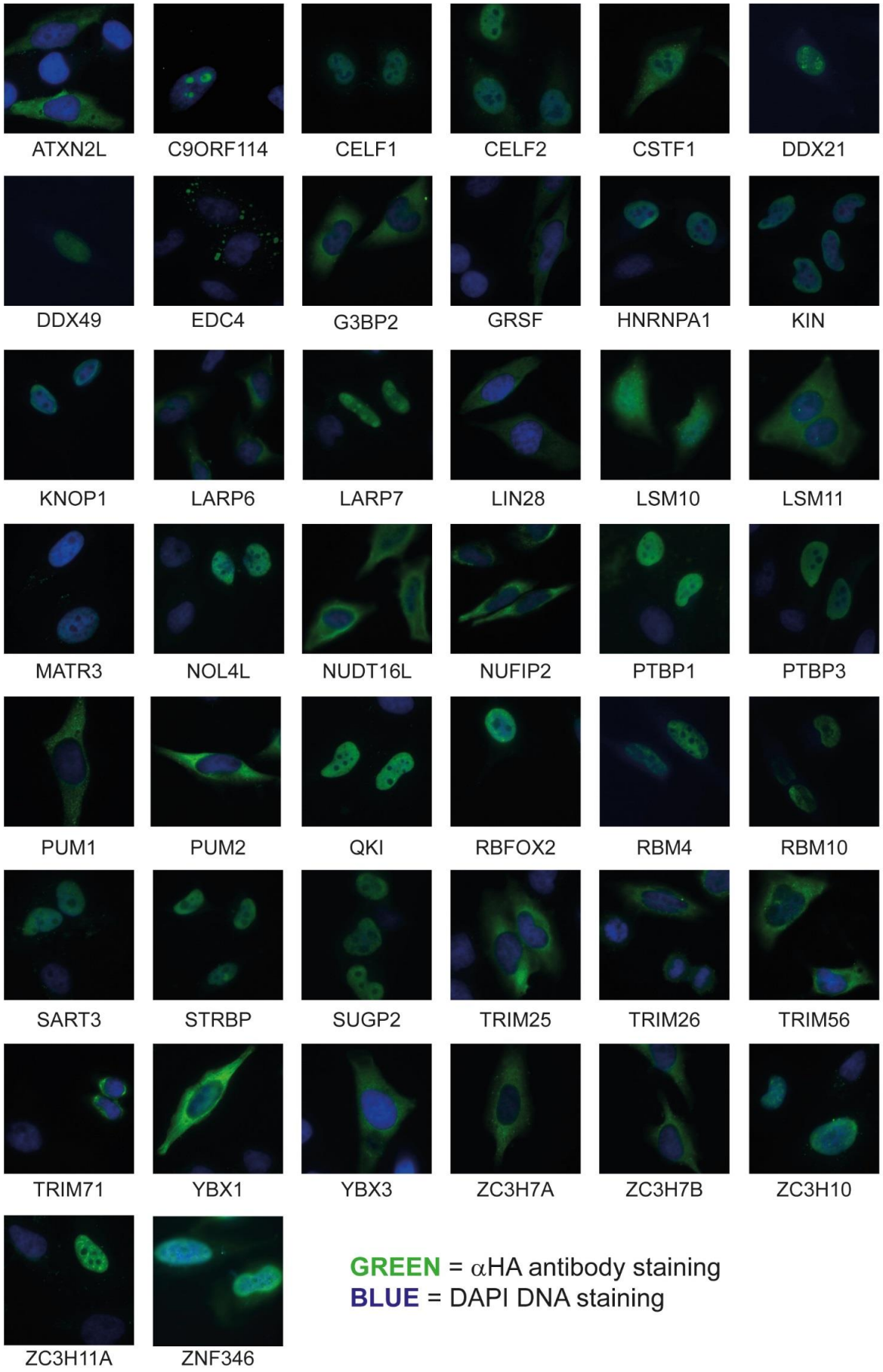

Figure S2 - related to Figure 2: for legend see previous page

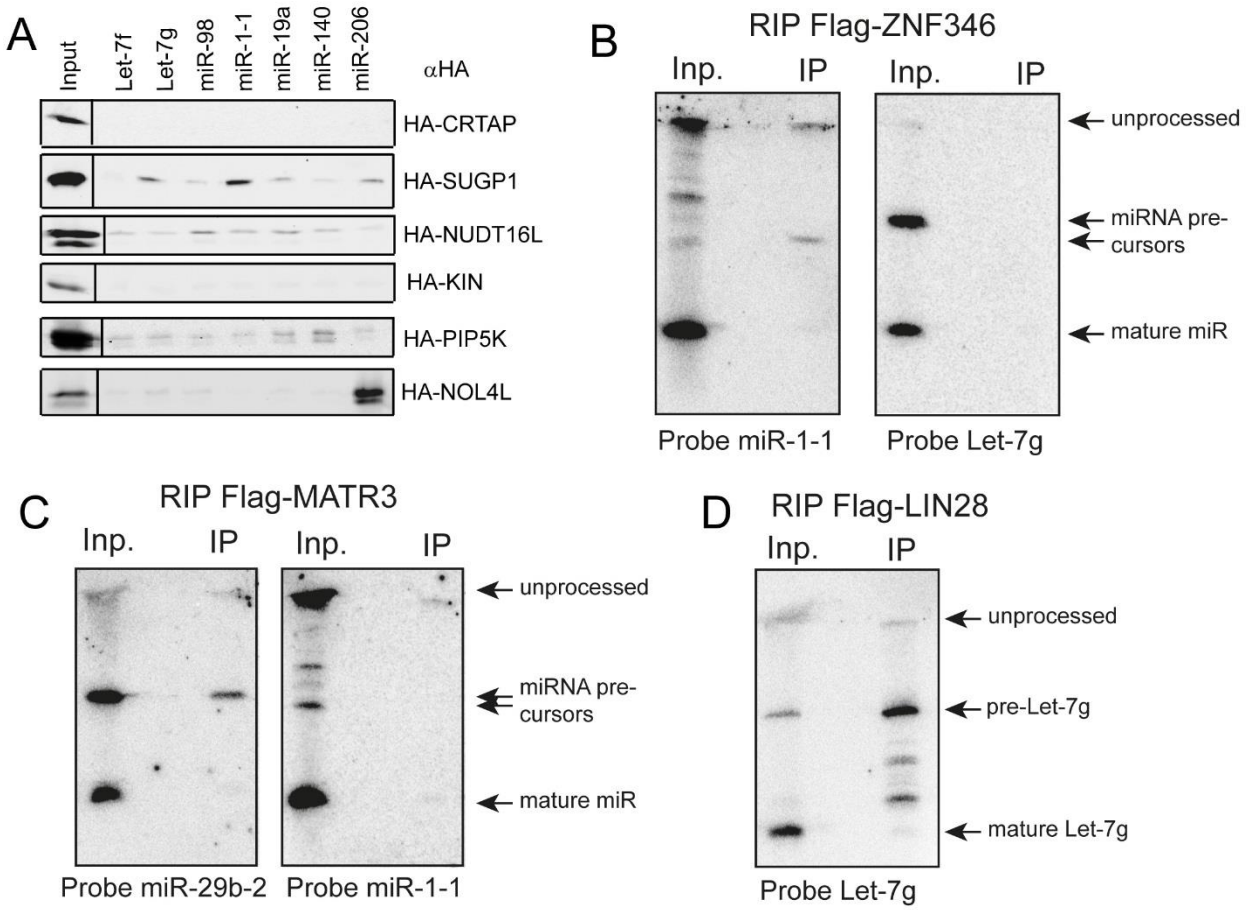

Figure S3 - related to Figure 3

A) Pull-down of overexpressed HA-tagged candidate proteins from cell lysate using the miRNA hairpins as indicated. Eluate fractions and 4% of input material are analyzed by immunoblot against the HA-tag.

B)-D) Northern blot analysis of RNA-IP experiments presented in Fig. 3C. Used probes and positions of miRNA processing intermediates are indicated.

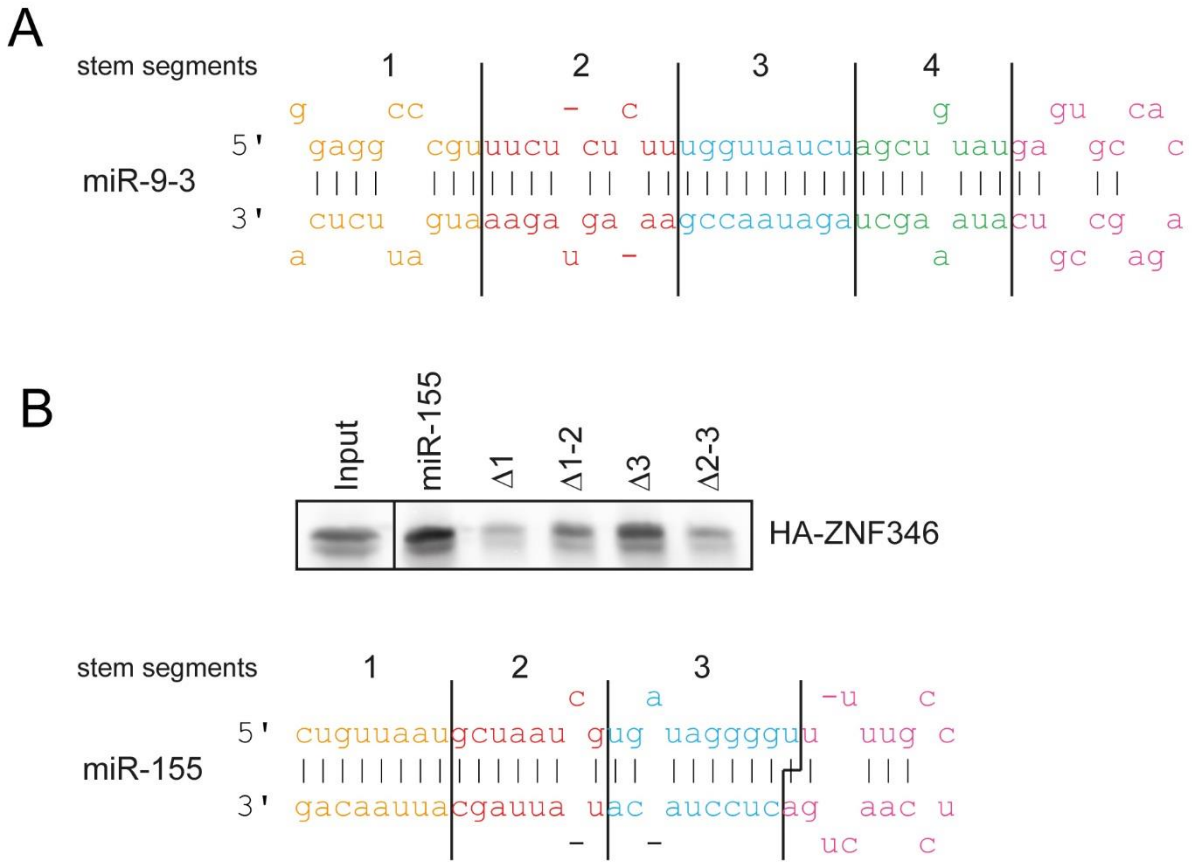

Figure S4 - related to Figure 4

A) Sequence representation of the miR-9-3 hairpin construct used in the pull-down assay. The four regions of the stem that were deleted for the mapping of the ZNF346 binding site in Figure 4E are marked in different colors and numbered.
B) Pull-down of overexpressed HA-ZNF346 from cell lysate using the miR-155 hairpin or variants containing deletions of stem segments as indicated. Eluate fractions and 4% of input material are analyzed by immunoblot against the HA-tag. The hairpin sequence and structure are shown and marked as in A).

Figure S5 (next page) - related to Figure 5

A) Northern blots of RNA from wildtype and PUM1-knockout HEK cells transfected with a mixture of pri-miR-199a-1 and pri-miR-143 expressing constructs. Transfections were performed in triplicate. The relative processing efficiency of both transcripts is determined by quantification of the mature miRNA signals and expressed as ratio of miR-199 over miR-143 for each cell sample. The quantitation is shown in Figure 5C.
B) Schematic representation of domains and sequence features in the ZC3H7A and ZC3H7B proteins.
C) Larger areas of northern blots shown in Figure 5I. Used probes are indicated. Migration of putative precursors is indicated by arrows.
D) Comparison of the contributions of the miR-15a/16-1 and miR-15b/16-2 pri-miRNA to the miR-16 level in HEK cells based on small RNA sequence reads of mature miR-15a-5p and mirR-15b-5p as well as the passenger strands miR-16-1-3p and miR-16-2-3p.
E) Relative quantitation of ZC3H7B-mRNA by qRT-PCR in the control knockdown and ZC3H7B knockdown samples shown in the northern blot in Fig. 5J.

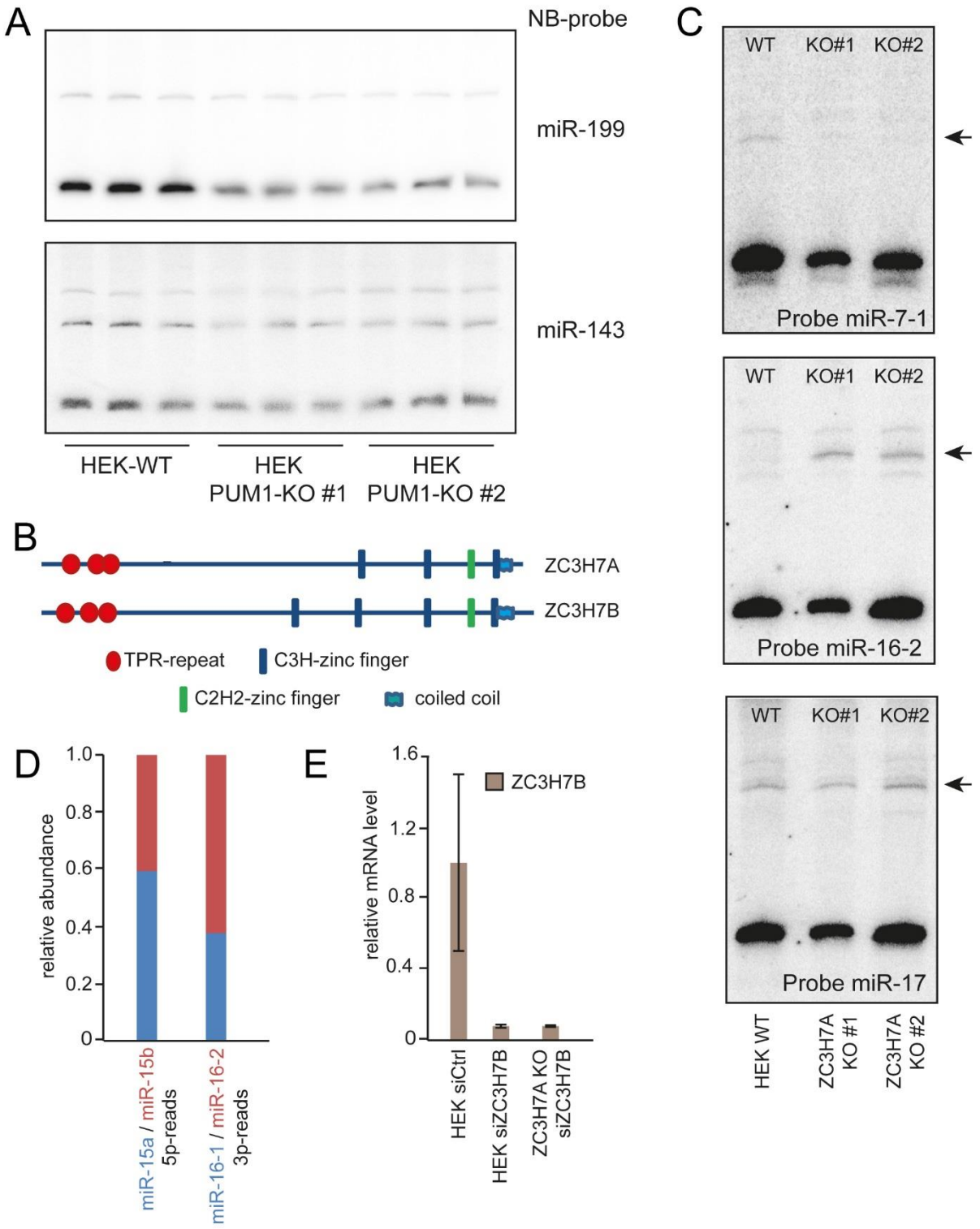

Figure S5 - related to Figure 5: for legend see previous page

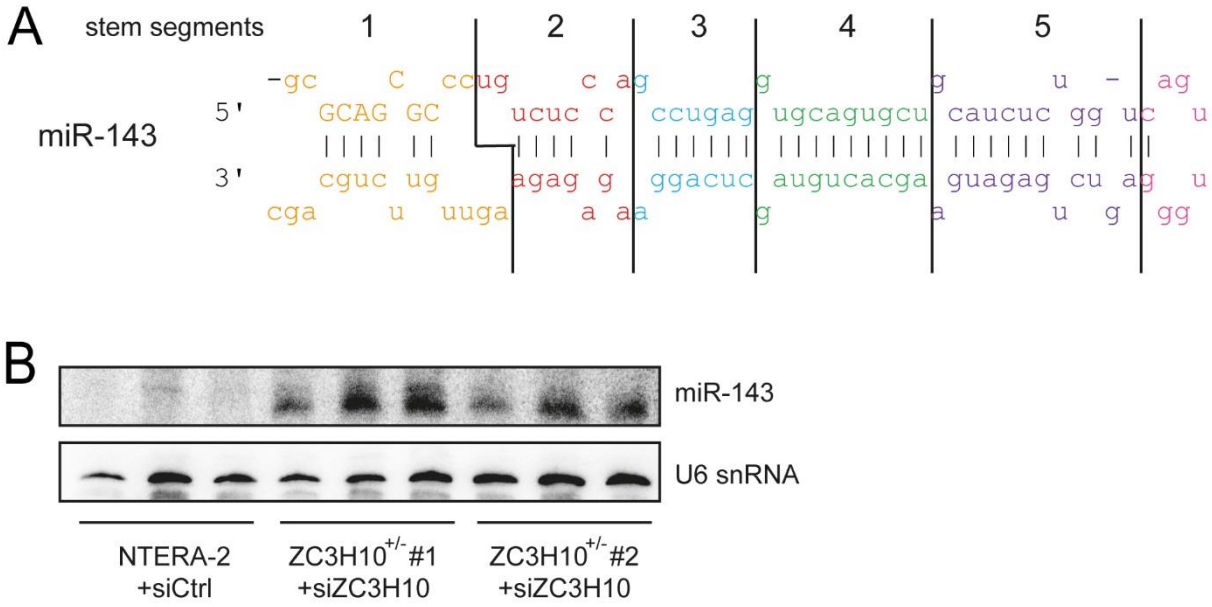

Figure S6: related to Figure 6

A) Sequence representation of the pri-miR-143 hairpin construct used in the pull-down assay. The five regions of the stem that were deleted for the mapping of the ZC3H10 binding site in Figure 6D are marked in different colors and numbered. The putative recognition motif of ZC3H10 is written in capital letters.
B) Northern blot analysis of endogenous miR-143 in NTERA-2 cells comparing wild type cells treated with control siRNA with heterozygous *ZC3H10*-knockout cells treated with ZC3H10 specific siRNA. A re-probed blot for U6 snRNA is shown as loading control.

Table S6: Genotypes of clones generated by CRISPR/CAS9-editing

Gene	Clone	Allele #	PCR-product	Reads
PUM1	**SK-N-MC KO #1 gRNA 1**	**WT**	GGACAAGACCAATGGTTTACCAGTGCAGAATGGGATTGATGCAGACGTCAAAGATTTTAG	**5300**
		1	GGACAAGACCAATGGTTTACCAGT-CAGAATGGGATTGATGCAGACGTCAAAGATTTTAG	**3200**
		2	GGACAAGACCAATGGTTTACCAGTG--GAATGGGATTGATGCAGACGTCAAAGATTTTAG	**2100**
	SK-N-MC KO #2 gRNA 1	**WT**	GGACAAGACCAATGGTTTACCAGTGCAGAATGGGATTGATGCAGACGTCAAAGATTTTAG	**5600**
		1	GGACAAGACCAATGGTT--------CAGAATGGGATTGATGCAGACGTCAAAGATTTTAG	**2500**
		2	GGACAAGACCAATGGTTTACCA----------TTGATGCAGACGTCAAAGATTTTAG	**3100**
	HEK KO #1 gRNA 1	**WT**	GGACAAGACCAATGGTTTACCAGTGCAGAATGGGATTGATGCAGACGTCAAAGATTTTAG	**3200**
		1	GGACAAGACCAATGGTTTACCAGTGATCGTGCTGACCCTGACACTGTTTGAGGACAGAGAGATGATCG	**3200**
	HEK KO #2 gRNA 1	**WT**	GGACAAGACCAATGGTTTACCAGTGCAGAATGGGATTGAT*GCAGACGTCAAAGATTTTAG*	**5500**
		1	GGACAAGACCAATGGTTTACCA-----GAATGGGATTGATGCAGACGTCAAAGATTTTAG	**1800**
		2	GGACAAGACCAATGGTTTACCAGT-CAGAATGGGATTGATGCAGACGTCAAAGATTTTAG	**1800**
		3	GGACAAGACCAATGGTTTACCAGTG--GAATGGGATTGATGCAGACGTCAAAGATTTTAG	**1800**
PUM2	**SK-N-MC KO #1 gRNA 1**	**WT**	GAATCATGATTTTCAAGCTCTTGCATTAGAATCTCGGGGAATGGGAGAGgtaaatgtttgcaaatactaag	**19700**
		1	GAATCATGATTTTCAAGCTCTTGCATTAGAATCTCGGGG--------AGGTAAatgtttgcaaatactaag	**6300**
		2	GAATCATGATTTTCAAGCTCTTGCATTAGAATCTCGGGG----------Tatgtttgcaaatactaag	**13300**
	SK-N-MC KO #2 gRNA 1	**WT**	GAATCATGATTTTCAAGCTCTTGCATTAGAATCTCGGGGAATGGGAGAGgtaaatgtttgcaaatactaag	**11500**
		1	GAATCATGATTTTCAAGCTCTTGCATTAGAATCTCGGG-AATGGGAGAGgtaaatgtttgcaaatactaag	**3300**
		2	GAATCATGATTTTCAAGCTCTTGCATTAGAAT----------GGGAGAGgtaaatgtttgcaaatactaag	**3400**
				4800
	HEK KO #1 gRNA 1	**WT**	GAATCATGATTTTCAAGCTCTTGCATTAGAATCTCGGGGAATGGGAGAGgtaaatgtttgcaaatactaag	**9200**
		1	GAATCATGATTTTCAAGCTCTTGCATTAGAATCTCGGGG----GGAGAGgtaaatgtttgcaaatactaag	**3900**
		2	GAATCATGATTTTCAAGCTCTTGCATTAGAATCTCGGGG----------taaatgtttgcaaatactaag	**5300**
	HEK KO #2 gRNA 1	**WT**	GAATCATGATTTTCAAGCTCTTGCATTAGAATCTCGGGGAATGGGAGAGgtaaatgtttgcaaatactaag	**11800**
		1	GAATCATGATTTTCAA----------aatgtttgcaaatactaag	**11800**
ZC3H10	**SK-N-MC +/- #3 gRNA 2**	**WT**	GGCAGCGAGGAGGCCAGTGGGGCAGGGGTAGGCAGTGGCGGGGCCAGCTCAGATGCCATCTGTA*GAGAC*	**11900**
		1	GGCAGCGAGGAGGCCAGTGGGGCAGGGGTAGGCAG----------CTCAGATGCCATCTGTAGAGAC	**3900**
		2	GGCAGCGAGGAGGCCAGTGGGGCAGGGGTAGGCAGTG----------ATCTGTAGAGAC	**5700**
		3	GGCAGCGAGGAGGCCAGTGGG----------GCGGGGCCAGCTCAGATGCCATCTGTAGAGAC	**2200**
	SK-N-MC +/- # 2 gRNA 1	**WT**	ATGCCTGACCGGGACAGCTATGCCAACGGTACCGGGAGCAGCGGTGGAGGCCCTGGAGGTGGTGGCAGCGAGG	**11800**
		1	ATGCCTGACCGGGACAGCTATGCCAAC----------GGAGGCCCTGGAGGTGGTGGCAGCGAGG	**4300**
		2	ATGCCTGACCGGGACAGCTATGCCAACGGTACCGGGA-CAGCGGTGGAGGCCCTGGAGGTGGTGGCAGCGAGG	**4500**
		3	ATGCCTGACCGGGACAGCTATGCCAACGGTACCGGG--CAGCGGTGGAGGCCCTGGAGGTGGTGGCAGCGAGG	**3000**

	SK-N-MC +/- #1 gRNA 1	**WT**	ATGCCTGACCGGGACAGCTATGCCAACGGTACCGGGAGCAGCGGTGGAGGCCCTGGAGGTGGTGGCAGCGAGG	**7850**
		1	ATGCCTGACCGGGACAGCTATGCCAACGGTACCGGGA-CAGCGGTGGAGGCCCTGGAGGTGGTGGCAGCGAGG	**4000**
		2	ATGCCTGACCGGGACAGCTATGCCAACGGTACCGGGAG---CGGTGGAGGCCCTGGAGGTGGTGGCAGCGAGG	**3850**
	NTERA-2 +/- # 1 gRNA 1	**WT**	ATGCCTGACCGGGACAGCTATGCCAACGGTACCGGGAG CAGCGGTGGAGGCCCTGGAGGTGGTGGCAGCGAGG	**5900**
		1	ATGCCTGACCGGGACAGCTATGCCAACGGTACCG---- ----------------GGAGGTGGTGGCAGCGAGG	**1900**
		2	ATGCCTGACCGGGACAGCTATGCCAACGGTACCGGGAG ----------AGGCCCTGGAGGTGGTGGCAGCGAGG	**2000**
		3	ATGCCTGACCGGGACAGCTATGCCAACGGTACCGGGAGGCAGCGGTGGAGGCCCTGGAGGTGGTGGCAGCGAGG	**2000**
	NTERA-2 +/- #2 gRNA 2	**WT**	ATGCCTGACCGGGACAGCTATGCCAACGGTACCGGGAGCAGCGGTGGAGGCCCTGGAGGTGGTGGCAGCGAGG	**11250**
		1	ATGCCTGACCGGGACAGCTATGCCAACGGTACCGGGAG----------GCCCTGGAGGTGGTGGCAGCGAGG	**5800**
		2	ATGCCTGACCGGGACAGCTATGCCAACGGTACCGGGAG----------CCCTGGAGGTGGTGGCAGCGAGG	**5350**
ZC3H7A	**HEK KO #1 gRNA 1**	**WT**	GTTTCTTCTTCTTAGGTCACCGCTGTCATATCCAGGAACACAGGAGCAATATGCGGTAATGACTCCGGG	**11900**
		1	GTTTCTTCTTCTTAGGTCACCGCTGTCATATCCAGGAA----------TATGCGGTAATGACTCCGGG	**8900**
		2	GTTTCTTCTTCTTAGGTCACCGCTGTCATATCCATAT-CACAGGAGCAATATGCGGTAATGACTCCGGG	**3000**
	HEK KO #2 gRNA 1	**WT**	GTTTCTTCTTCTTAGGTCACCGCTGTCATATCCAGGAACACAGGAGCAATATGCGGTAATGACTCCGGG	**13500**
		1	GTTTCTTCTTCTTAGGTCACCGCTGTCATATCCAGGA--------GCAATATGCGGTAATGACTCCGGG	**4500**
		2	GTTTCTTCTTCTTAGGTCACCGCTGTCATATCCAGG--CACAGGAGCAATATGCGGTAATGACTCCGGG	**4300**
		3	GTTTCTTCTTCTTAGGTCACCGCTGTCATATCCAGGAA--CAGGAGCAATATGCGGTAATGACTCCGGG	**4700**
TRIM71	**NTERA-2 KO #1 gRNA 1**	**WT**	GCTGCTGCTCCGCCGTCCTCACGGCTGCAGCTCGTGCGA TGAGGGCAACGCAGCTTCTTCGCGCTGC	**2150**
		1	GCTGCTGCTCCGCCGTCCTCACGGCTGCAGCTCGTGCGATTGAGGGCAACGCAGCTTCTTCGCGCTGC	**2140**
	NTERA-2 KO #2 gRNA 2	**WT**	CCCAAGAACGGGCGCGCCGGCGCTCCGGCGGG AGCGGGCGGCCACAGCAACC	**2500**
		1	CCCAAGAACGGGCGCGCCGGCGCTCCGGCGGGCCAAGGTCGCACAGCAAATGGCAGAGCCAGACACTCAAACTTGTGAGCGGGCGGCCACAGCAACC	**2300**

Alignment of wild type sequence of gRNA-target loci with edited variants as identified by deep sequencing are shown. The gRNA target site is highlighted in red. Deletions in the edited alleles are marked as blue dashes, insertes nucleotides are given in blue print. Exonic sequence is given in capital letters, intronic sequence is shown in lower case. The “reads” column gives the number of total reads of the locus identified in the respective clone as underlined number, the fraction that corresponds to the different alleles is indicated below. Read numbers shown in red correspond to alleles without a nonsense mutation.